NUSC Technical Document 8559
8 January 1990

(4)

A Preliminary Analysis of Threshold Signal Detection in Ambient and Signal-Dependent Noise Environments

Weapon Systems Technology & Assessment Department

Naval Underwater Systems Center
Newport, Rhode Island/New London, Connecticut

Preface

This document was prepared for the Weapon Systems Technology & Assessment Department by Dr. David Middleton of Sonalysts, Inc., under Contract N66604-87-D-0546-0031.

Reviewed and Approved: 8 January 1990

F. L. White
Head, Weapon Systems Technology & Assessment Department

Unclassified
SECURITY CLASSIFICATION OF THIS PAGE

REPORT DOCUMENTATION PAGE

1a. REPORT SECURITY CLASSIFICATION Unclassified	1b. RESTRICTIVE MARKINGS
2a. SECURITY CLASSIFICATION AUTHORITY	3. DISTRIBUTION/AVAILABILITY OF REPORT Approved for public release; distribution unlimited
2b. DECLASSIFICATION/DOWNGRADING SCHEDULE	
4. PERFORMING ORGANIZATION REPORT NUMBER(S) TD 8559	5. MONITORING ORGANIZATION REPORT NUMBER(S)
6a. NAME OF PERFORMING ORGANIZATION Naval Underwater Systems Center 6b. OFFICE SYMBOL (If applicable) Code 8219	7a. NAME OF MONITORING ORGANIZATION
6c. ADDRESS (City, State, and ZIP Code). Newport Laboratory Newport, RI 02188	7b. ADDRESS (City, State, and ZIP Code)
8a. NAME OF FUNDING/SPONSORING ORGANIZATION 8b. OFFICE SYMBOL (If applicable) Code 8219	9. PROCUREMENT INSTRUMENT IDENTIFICATION NUMBER
8c. ADDRESS (City, State, and ZIP Code)	10. SOURCE OF FUNDING NUMBERS PROGRAM ELEMENT NO. / PROJECT NO. / TASK NO. / WORK UNIT ACCESSION NO.

11. TITLE (Include Security Classification)
A Preliminary Analysis of Threshold Signal Detection in Ambient and Signal-Dependent Noise Environments

12. PERSONAL AUTHOR(S)
David Middleton

13a. TYPE OF REPORT	13b. TIME COVERED	14. DATE OF REPORT (Year, Month, Day)	15. PAGE COUNT
Tech. Doc.	FROM 7/1988 TO 2/1989	1990 January 8	

16. SUPPLEMENTARY NOTATION

17. COSATI CODES			18. SUBJECT TERMS (Continue on reverse if necessary and identify by block number)
FIELD	GROUP	SUB-GROUP	Threshold Signal Detection; Signal-Dependent Noise, Reverberation, Scattering, Target Modeling, Doppler Effects Wave Surface Scatter, Optimum Performance

19. ABSTRACT (Continue on reverse if necessary and identify by block number)

Weak signal detection of signals scattered by ocean wave surfaces and reflecting bodies is examined. Optimum threshold algorithms, as extensions of earlier work [1], [2], [5], [10], are determined, which contain in addition to the usual ambient background noise, signal-dependent noise generated in the scattering process. Threshold performance probabilities are formulated, in terms of the now-generalized performance parameters associated with coherent and incoherent detection. As before, a canonical theory is presented, which is invariant of specific noise statistics and signal waveforms. Both spatial and temporal processing are included, the former implicitly in many cases by means of projected beam patterns.

The physico-geometrical factors of platform motion, beam patterns, distributed scattering elements and source and receiver geometries for both the "monostatic" and "bistatic" regimes are summarized. Various distributed target models are presented, including quasi-phenomenological ones capable of analytic evaluation, involving both

20. DISTRIBUTION/AVAILABILITY OF ABSTRACT ☐ UNCLASSIFIED/UNLIMITED ☒ SAME AS RPT. ☐ DTIC USERS	21. ABSTRACT SECURITY CLASSIFICATION Unclassified
22a. NAME OF RESPONSIBLE INDIVIDUAL Mr. James Kelly	22b. TELEPHONE (Include Area Code) (401) 841-4558 22c. OFFICE SYMBOL Code 8219

DD FORM 1473, 84 MAR 83 APR edition may be used until exhausted. All other editions are obsolete.

SECURITY CLASSIFICATION OF THIS PAGE
Unclassified

Block 19, continued:

continuous and discrete scatterers. Under the present condition of narrow-band signals and far-field geometries, the input signal waveforms are explicitly separable from these physico-geometric factors. A "weak" target is assumed, in "weak reverberation," vis-à-vis strong ambient noise.

Sufficiently detailed analytic structure is provided, along with the availability of [5], to achieve explicit, quantitative results, and to guide the treatment of special problems. A short list of possible next steps is included.

A Preliminary Analysis of Threshold Signal Detection in Ambient and Signal-Dependent Noise Environments

Table of Contents

List of Principal Symbols: (See also Appendix A.1 and [5])

$A_o, \tilde{A}_o$	=	peak signal amplitudes, (2.1b), (3.1a)
$a_{on}^{(m)}, a_o, a_{on}, \tilde{a}_o$, etc.	=	input signal-to-noise (amplitude) ratios; (to receiver); to medium, $\tilde{a}_o$,
$\underline{\varrho}_o, \underline{\varrho}_{oT}, \underline{\varrho}_{o\beta T}, \underline{\varrho}_{o\beta R}$	=	directional vectors
$\alpha_F^{(*)}$	=	false alarm probability
α_H, α_I	=	direct and scattered wave fields
$\mathcal{A}_T, \mathcal{A}_R, \mathcal{A}_\beta$	=	beam patterns, or beam pattern projections
$B_J^{(*)}$-coh, inc	=	detector bias terms
$B_o^{(s)}(t)$	=	waveform factor, due to wave surface scattering
$B_o^{(\tau)}(t)$	=	waveform factor, due to target scattering
$\varepsilon, \varepsilon_o$	=	epochs
f_o	=	carrier frequency
F_l	=	characteristic function
$g_J^{(*)}$	=	threshold detection algorithms
$H_0, H_1, H'_2, H'_1,$	=	hypothesis states, in detection
$\hat{\imath}_x, \hat{\imath}_{x'}$, etc.	=	unit vectors
$J = MN$; $j = m,n$	=	space-time (sample) indexes
k_o, k	=	(angular) wave numbers
$\hat{K}_o(\tau)_{in}$	=	signal correlation function
l, l_n, l'	=	nonlinear detector transfer function
$L^{(2)}, L^{(4)}$	=	(nongaussian) noise statistics
$l_1, l_2, l_3,$	=	direction of cosines (x)
μ	=	p/q: ratio of a priori data probabilities
m_1, m_2, m_3	=	direction of cosines (y)
n_1, n_2, n_3	=	direction of cosines (z)
n_R, n_A	=	normalized (received) noise processes
η	=	field renormalization operator
$\hat{n}$	=	surface normal
$\underline{\gamma}, \underline{\gamma}_{o\beta}, \underline{\gamma}_{oT}, \underline{\gamma}_T$, etc.	=	wave numbers (associated with beam patterns)
ψ	=	(received) nongauss + gauss noise intensities
ω_o	=	$2\pi f_o$ = angular carrier frequency
R	=	receiving array operator
$R_o, R_{o\beta}$	=	(plane-wave) reflection coefficients
$s(t), \hat{S}_o(t)_{in}, St$	=	input signal waveforms
$\sigma_{oJ}^{(*)}$	=	detection performance parameter
S	=	shadowing function

τ	= $t_2 - t_1$
Θ	= error function
θ, $\theta_{m,n}$, θ_n	= normalized received signals
$\theta^{(s)}$, $\theta^{(\tau)}$	= normalized received scatter "signals," target signals
v_D, Δv_D	= doppler velocities
w_1	= noise probability density
$W_{RT\text{-}\beta}$, $w_{RT\text{-}\beta}$, $w_{RT\text{-}s}$	= wave number spectra, target and wave scattering surface
ζ	= wave surface elevation

List of Figures

A Preliminary Analysis of Threshold Signal Detection in Ambient and Signal-Dependent Noise Environments

by

David Middleton

1. Introduction

This document extends the earlier work of the author ([1], and refs. therein) for the space-time extraction of weak signals in general nongaussian noise to include signal-dependent noise, i.e., reverberation, and distributed targets, in an underwater acoustic environment. Although this is a venerable problem, analogous to radar target detection in ground clutter, for example, recent analysis, incorporating statistical-physical models of general nongaussian ambient noise mechanisms [2]–[4] and detailed scattering treatments which contain the relevant geometrical and physical features [5], [6], can now be applied and generalized to this class of problem where a significant component of the interfering noise is signal-dependent, as well as often nongaussian.

In addition, the results of this study provide a framework for obtaining potential improvement of these active systems by means of "signal design," whereby a subclass of signal waveforms (subject to suitable constraints) may be found which further reduce the probabilities of decision error in system performance [7]. The extension of these results in turn can lead to a possible. more restricted, class of "low-probability intercept" (LPI) signals, dependent upon the physical constraints involved [8].

As before [1], [9]–[11], except in specific examples, the treatment is generally canonical, in the sense that the functional *form* of the results is invariant of specific signal and noise models and statistics, as well as specific physical circumstances, geometries, etc. Fortunately, this is always possible in threshold-signal theory [10], [11], which in turn permits direct application to a very wide spectrum of practical situations. The particular physical environment, of course, provides the needed quantitative calibration to the canonical results [1]. [2], [9], [12]. Finally, although the analytic emphasis here is on optimum algorithms, practical sub- or "near-optimum" procedures can be readily derived from, and compared with, the former [8]–[10]. It is these which are usually the economical ones to implement.

1.1 New Features

Most of the elements of our present analysis have become available during the last decade. What is the principal new feature here is their combination in a single formalism which permits the controlling details of the physical environment to appear in a realistic, i.e., statistical-physical way. This will become explicitly evident in succeeding sections. Also, because detailed derivations of many of the components of our treatment are available in the recent literature ([1], [3], [9]–[12] and refs. therein), we shall not provide them here, other then by reference. What are these needed elements? They are, concisely:

I. *Nongaussian Noise Backgrounds*, with more or less significant gaussian components;

II. *Ambient and Signal-Dependent Noise*: ocean *ambient noise* often has significant nongaussian components, e.g., biological sources, shipping, and structural noise, produced, for example, by arctic ice [13]–[15], in the course of its local motion.

III. *Distributed Targets*: these produce signal-dependent returns, of course, which consist of both resolvable and unresolvable "multipath" effects, dependent partially on the (partially) random orientation of the reflecting elements. In these acoustic cases we may also expect mechanical resonance effects, excited by the incident radiation, which can be a significant feature of the target structure. Here we shall introduce some comparatively simple quasi-phenomenological target models, whose numerical evaluations require empirical data [cf. Sec. 4.4 ff.].

IV. *Doppler Effects*: these arise because of the relative motion between source and target, which includes both deterministic and random components. Because the speeds involved are small compared to the (group) velocity (c_0) of sound in the ocean, e.g., $|v_D| << c_0$, a manageable analytic theory is possible [17]. For any realistic treatment doppler effects must be included here.

V. *Explicit Geometries*: quantitatively, source, target, and boundary geometries play a critical rôle in practical signal detection and design problems [1], [5], [8], particularly in our present class of problem, as is analytically evident here, cf. Secs. 3.5 ff.

VI. *Physical Models*: these also play critical rôles in our analyses since they determine the (generally) statistical description of the various ambient and scattering noise and signal mechanisms in the course of propagation in the medium ([1], [2], [5], for example). Moving wind-wave surfaces, ocean bottom elevations, distributed targets, etc., are essential mechanisms here.

All the above have received detailed attention, recently and earlier [cf. [1], [5], and remarks, refs.]. Our principal task, as noted earlier, is to combine the relevant elements of I–VI above, to obtain the "macro-algorithms," so to speak, and their expected performance measures, viz. here,

probabilities of correct decisions, in such a way as to incorporate the controlling physical factors which the acoustical environment here imposes.

1.2 The Basic Geometry

Figure 1.1 shows in a symbolic way the governing geometry for the class of problems examined in this study. A general "bi-static" geometry is sketched in Fig. 1.1a, while Fig. 1.1b shows a typical "monostatic" configuration. The directional lines represent effective directions of both coherent and incoherent, direct, and scattered radiation ([1], Fig. 2). For the present we shall ignore volume scatter and the effects of velocity gradients ($\nabla c \neq 0$) in the medium. This restricts us to comparatively short ranges. Also, we shall assume configurations where bottom scatter, if any, is quite separable from target and wave surface returns, and can therefore be disregarded here. All these features can, of course, be included in the same way we approach the problems conforming to the geometries of Fig. 1.1: the results are simply formally, not conceptually, more complex.*

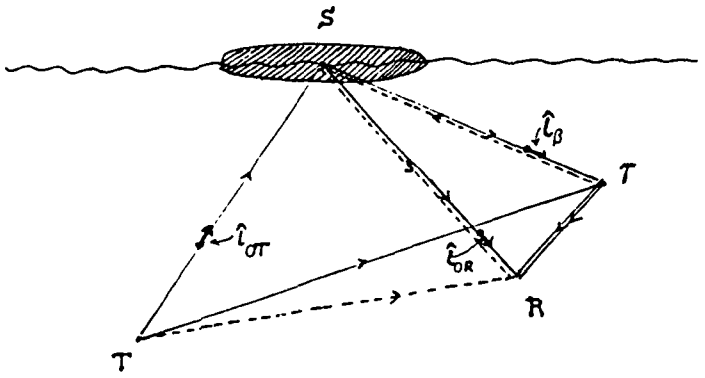

Fig. 1.1a: "Bistatic" Régime: direct path and multipaths to targets; surface "forward" scatter ($\nabla c = 0$).

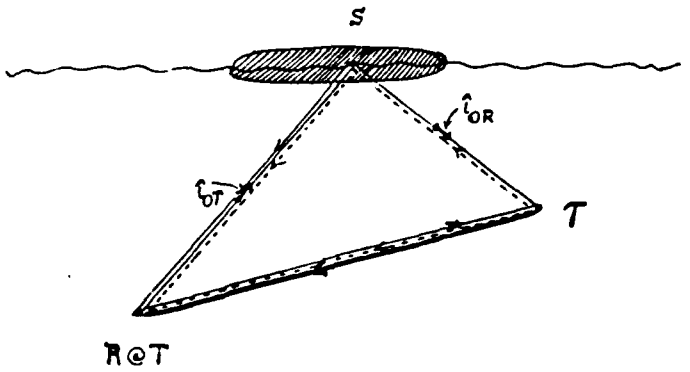

Figure 1.1b: "Monostatic" Régime: direct path and multipaths to target; surface and target backscatter ($\nabla c = 0$).

* This is not entirely true for the longer-range cases where $\nabla c \neq 0$ must be accounted for. See [18].

1.3 Aims and Organization

Our aims here may be concisely stated: they are

A. To obtain threshold detection algorithms for scattered signal returns in signal-dependent (reverberatory) noise, as well as ambient noise backgrounds, when the latter are strong vis-à-vis the former;

B. To predict the performance of these threshold algorithms, in terms of probabilities of correct decisions; and

C. From the results of A and B, to indicate an approach to signal design, with appropriate physical constraints.

As stated earlier, the analysis is directed to *optimum systems* (in the Bayesian sense, Chapter 18 of [7]), whose structures are to be approximated by practical, or "near-optimum" algorithms, which in turn are usually the candidates for implementation.

The Report is organized as follows:

i. Section 2 provides a concise summary of the threshold detection formalism extended now to include signal-dependent noise;

ii. Section 3 assembles various signal-dependent (reverberation) noise results, appropraite to the scenarios of Fig. 1.1, while

iii. Section 4 introduces some quasi-phenomenological target models, whose distributed nature is specifically noted, along with a resonant component.

iv. Secton 5 contains a short summary of the "telecommunication" or direct path cases, where the target is capable of detecting the emitted signal.

v. In Section 6, the rôle of performance measures is discussed, including the relevent physical parameters of the detection scenario.

vi. In addition in Section 6, the Report concludes with a short critique of the approach and results, along with suggested next steps.

For technical details and derivations the reader is referred in most instances to the indicated references. Reference [5], in paritcular, will be needed here also, for many definitions and descriptions, in order to avoid an excessively lengthy treatment. Reference [5] is recommended as a companion document for the detailed applications of this study.

2. Threshold Signal Detection in Ambient and Reverberatory Noise: Canonical Structures

Here we summarize some of the principal results needed in out current detection situation. which include space-time operation. We begin with

2.1 Threshold Detection Algorithms [1]

There are three principal forms of optimum (and suboptimum) threshold detection algorithms, depending on the receiver's *a priori* state of information. These are [1], Sec. VII:

I. Coherent Detection

In this case, signal epoch (ε_o) is known precisely at the receiver, so that appropriate cross-correlation with the received signal is possible. The corresponding (optimum) algorithm is

$$g_J^*(x) = B_{J\text{-}coh}^* - \sum_{m,n}^{J} l_{m,n}\langle\theta_{m,n}\rangle, \tag{2.1}$$

where

$$l_{m,n} = \frac{d}{dx}\log w1(x)]_{x_{m,n}};\ x_{m,n} = x(t_n|r_m), \tag{2.1a}$$

and $x_m = [x_{m1}, ..., x_{mn}, ..., x_{mN}]$ is the (normalized) data sample at the m^{th} sensor, $x_j = X_j/\sqrt{\Psi}$, with $x = [x_m]$, m = 1, ..., M sensors; here J = MN is the total number of space-time samples. The quantity $\theta_{m,n}$ is a signal-to-noise ratio, also normalized, such that

$$\theta_{m,n} = a_o^{(m)}(t_n)s^{(m)}(t_n) = a_{on}^{(m)}s_n^{(m)2};\ \langle s_n^{(m)}\rangle_t = 1;\ \text{(all n), each m.} \tag{2.1b}$$

and $a_{on}^{(m)} = A_{on}^{(m)}/\sqrt{2\Psi}$, where $A_{on}^{(m)}$ = peak signal value = $A_n^{(m)}(t_n)$ and ψ = sum of the intensities of the ambient, *signal-independent* noise accompanying the signal, including system noise in the receiver. $B_{J\text{-}coh}^*$ is a *bias term*, cf. (2.15a,b) ff.; also, (64), (66a) of [1]. Here < > denotes a (statistical) average over any ramdom parameters.

In our present formulation we postulate *independent sampling*. [This can be realistic for time-sampling and not so closely approximated for spatial sampling. Analytically, very considerable simplification is thereby introduced, see [11], m Sec. 10, especially.] Thus, the pdf $w_1(\mathbf{x})$ of the data vector **x** reduces to $\prod_{j=1} w_1(x_j)$, j = mn = 1, ..., J, where $w_J(\mathbf{x})$ is the first-order pdf of the space-time, *here signal-independent noise* process **x**, cf. (2.1a) above.

As we see presently, θ can include a signal-dependent noise term, cf. (2.10)-(2.12), which includes, as expected, the reverberatoray or scatter component form boundaries and volume inhomogeneities, and the possible target, when all are weak vis-à-vis the signal independent noise contributions.

The important class of suboptimum detectors associated with $g_{J\text{-}coh}^*$, (2.1), here are those for which some simple approximation h(x) of l(x), (2.1a), is employed, for example, strong "clippers," when highly impulsive (ambient) noise is the dominant interference ([10]; [19], Sec. 9). Thus, the corresponding form of threshold detector to (2.1) becomes

$$g_J(x)_{coh} = B^*_{J\text{-}coh} - \sum_{m,n} h_{m,n} \langle \theta_{m,n} \rangle, \quad h_{m,n} = h(x)|_{x=x_{m,n}}. \tag{2.2}$$

(The same bias is used in (2.1), (2.2), to insure that as $h \to l$, $g_J \to g^*_J$.)

II. Incoherent Detection Algorithms [1]

This "incoherent" case is distinguished by the complete lack of knowledge of signal epoch (ε_0) at the receiver, so that $\langle\theta\rangle = \langle\theta(\varepsilon_0, \ldots)\rangle_{\varepsilon_0,\ldots} = 0$. The appropriate threshold algorithm here is found to be ((60), [1])

$$g^*_J(x)_{inc} = B^*_{J\text{-}inc} + \frac{1}{2!} \sum_{mm'nn'} [l_{m,n} l_{m',n'} + l'_{m,n} \delta_{mm'} \delta_{nn'}] \langle \theta_{m,n} \theta_{m',n'} \rangle, \tag{2.3}$$

where now

$$\langle \theta_{m,n} \theta_{m',n'} \rangle = \overline{a_0^2}\, \hat{m}^{(m,m')}_{|n-n'|}\, \rho^{(m,m')}_{n-n'}, \text{ with} \quad \left.\begin{aligned} \hat{m} &\equiv \overline{a^{(m)}_{on} a^{(m')}_{on}} \,/\, \overline{a_0^2}\,, && (2.3a)\\ \rho &\equiv \langle s^{(m)}_n s^{(m')}_{n'} \rangle && (2.3b)\\ l'_{m,n} &= \frac{dl}{dx}\Big|_{x_{m,n}}\,. && (2.3c) \end{aligned}\right\}$$

The quantities $\hat{m}$ and ρ are respectively amplitude and (normalized) waveform correlation functions associated with the input signal, either directly or functionally, as we shall see below in Secs. 3, 4; $\overline{a_0^2}$ is an input signal-to-(ambient) noise ratio. Generally $\hat{m}$ contains any fading effects, while ρ is influenced by "doppler-smear," which is primarily a phase (or frequency) modulation mechanism, cf. (63), [4]. For the corresponding class of simpler (sub-optimum) detectors $l(x)$ is again repleaced by $h(x)$, cf. (2.2).

III. Composite Detection Algorithms [9]–[11]

This is the most general threshold formulation, which takes advantage of both coherent and incoherent information about the received signal and noise. In fact, by derivation it is simply the sum of the coherent and incoherent algorithms (minus an *a priori* bias correction), viz.:

$$g^{(*)}_{J\text{-}comp} = g^{(*)}_{J\text{-}coh} + g^{(*)}_{J\text{-}inc} - \log \mu, \quad \text{(cf. Eq. (2.2c), [9])}, \tag{2.4}$$

where $\mu = p/q$ = ratio of the *a priori* probabilities of there being the desired signal in the data x. In this way any coherent signal structure can be used, in addition to the associated incoherent structure, further to enhance the performance of the latter.

2.2 The Decision Situation: Signal-Dependent Noise

Using Section III, IV of [1] let us describe the decision situation where now signal-dependent noise is included. Since the medium involved is linear, this is formally done in a straightforward fashion. We have, for the two hypothesis stated here, in these binary detection situations at the receiver:

$$\begin{cases} H_1: S \oplus N: & X = N_R + N_A + S + S_{scat} \quad (2.5a) \\ & \text{vs.} \\ H_0: N: & X = N_R + N_A + S_{scat}, \quad (2.5b) \end{cases}$$

where N_R, N_A are respectively independent receiver and (received) ambient noise, S represents the desired signal, while S_{scat} is received signal-dependent noise *not* associated with any desired target. For the régimes of Fig. (1.1) we see that for the desired signal

$$S_\tau = (S_\tau)_{direct} + (S_\tau)_{multipath}, \quad (2.6a)$$

where $(S_\tau)_{multipath}$ has different components:

$$\left.\begin{array}{ll} \textit{Monostatic (Fig. (1.1b)}: & [(S_\tau)_{multipath} = S_{T\to S\to\tau\to R} + S_{T\to\tau\to S\to R}]_{mono}; \quad (2.6b) \\ \textit{Bistatic (Fig. (101a)}: & [(S_\tau)_{multipath} = S_{T\to S\to\tau\to R} + S_{T\to\tau\to S\to R}]_{bi}. \quad (2.6c) \end{array}\right\}$$

Similarly, we find that for the interface (S) and volume (V) scatter that

$$\left.\begin{array}{ll} \textit{Monostatic (Fig. (1.1b)}: & (S_{scat} = S_{T\to S\to R} + V_{T\to R})_{mono}; \quad (2.7a) \\ \textit{Bistatic (Fig. (1.1a)}: & (S_{scat} = S_{T\to S\to R} + V_{T\to R})_{bi}. \quad (2.7b) \end{array}\right\}$$

Of course, the contribution of each term in (2.6), (2.7) is different because of the different geometries involved. All of the components are signal-dependent.

However, not all target and scatter terms are comparable. Even for rather general geometries the multiple interactions with the random interface (S) considerably reduces the effective return to the receiver. Accordingly, in the first order we can disregard $(S_T)_{multipath}$. Moreover, since the interaction with wave surface (S) [or bottom (B), not considered here] is normally much stronger than from the volume inhomogeneities in these geometries where the surface is at ranges comparable to the target (τ), we can ignore volume effects, so that (2.6b,c), (2.7) are replaced by

$$(S_\tau)_{\text{multipath}} \cong 0; \quad S_{\text{scat}} \cong S_{T\to S\to R} \tag{2.8a}$$

and (2.6b) reduces to

$$\therefore (S_\tau) = (S_\tau)_{\text{direct}} . \tag{2.8b}$$

Consequently, the decision situation (2.5a,b) also reduces to

$$\boxed{\begin{array}{ll} H_1\text{: } S \circledast N\text{:} & \mathbf{X} \cong N_R + N_A + (S_\tau)_{\text{direct}} + S_{T\to S\to R} \\ & \text{vs.} \\ H_0\text{: } N\text{:} & \mathbf{X} = N_R + N_A + S_{T\to S\to R} . \end{array}} \tag{2.9}$$

The ambient noise N_A and receiver noise N_R cannot be ignored: they are always present and set the ultimate limit on threshold performance, whereas S_τ and S_{scat} vanish as $S_{\text{in}} \to 0$ at the source (T). Our rather detailed passage from Eqs. (2.5) to Eq. (2.9) is justified here on the grounds that it is necessary to separate the present, quite common cases embodied in (2.9) from the other, more complex and rarer ones which at some later point it will be necessary to consider.

Next, in normalized form, consistent with the results of Sec. 2.1 above, we can rewrite (2.7) as

$$\left.\boxed{\begin{array}{ll} H_1\text{: } (s_2 \circledast n\text{:}) \to H_2'\text{:} & \mathbf{x} \cong n_R + n_A + \theta^{(\tau)}_{\text{direct}} + \theta^{(s)}_{(T\to S\to R)} \\ \text{vs.} & \\ H_0\text{: } (s_1 \circledast n\text{:}) \to H_1'\text{:} & \mathbf{x} \cong n_R + n_A + \theta^{(s)}_{(T\to S\to R)} , \end{array}}\right\}^{\circledast} \tag{2.10}$$

with $\theta^{(s),(\tau)} = \theta(S_{\text{in}})$, e.g., θ is *linear* source function (or functional)* of the transmitted signal S_{in}. Here, specifically,

$$\mathbf{x} = \mathbf{X}/\sqrt{\psi}; \; n_R = N_R/\sqrt{\psi}; \; n_A = N_A/\sqrt{\psi}; \; \psi \equiv \langle N_A^2 \rangle + \langle N_R^2 \rangle , \tag{2.10a}$$

and

$$\boxed{S = \sqrt{\psi}\,\theta .} \tag{2.10b}$$

It is important to note that, *in essence, the scattered return is treated as just another signal,* albeit a

* This follows at once from the fact that the medium and scatter process are linear, cf. Eqs. (14) and (18) of [1].

⊛ add θ_{direct} to (2.10) for bi-static cases; θ_{direct} omitted in analysis here.

random one, generally. *The formal effect of this is to allow us to replace* θ *by* $\theta^{(\tau)} + \theta^{(s)}$ *in all our earlier results involving signal-independent noise,* where now, of course, the appropriate physical structure of $\theta^{(\tau)}$ and $\theta^{(s)}$ must be incorporated. Formally, the signal ($S^{(\tau)}$) or noise (H_1 vs. H_0) is replaced by an artificial binary *two-signal situation*, H_2' vs. H_1', cf. (2.10), where $\theta_1 \equiv \theta^{(s)}$ and $\theta_2 \equiv \theta^{(s)} + \theta^{(\tau)}$. For these cases of weak targets and weak reverberation in strong nongaussian noise, the threshold algorithms (2.1), (2.3) are at once modified according to:

I. Coherent Detection:

$$< \theta_{m,n} > \rightarrow < \theta^{(2)}_{m,n} > = < \theta^{(\tau)}_{m,n} > + < \theta^{(s)}_{m,n} >, H_2', \text{ vs } < \theta^{(1)}_j > = < \theta_{m,n} > \rightarrow < \theta^{(s)}_{m,n} >, H_1'; \tag{2.11}$$

II. Incoherent Detection:

$$< \theta_{m,n}\theta_{m',n'} > \rightarrow < \theta^{(\tau)}_j \theta^{(\tau)}_{j'} > + < \theta^{(s)}_j \theta^{(s)}_{j'} > + < \theta^{(\tau)}_j \theta^{(s)}_{j'} > + < \theta^{(\tau)}_{j'} \theta^{(s)}_j >, H_2', \text{ vs.}$$
$$< \theta^{(\tau)}_j \theta^{(\tau)}_{j'} > \rightarrow < \theta^{(s)}_j \theta^{(s)}_{j'} >, H_1'; \qquad j = mn,\ j' = m'n', \tag{2.12}$$

where due account must be taken of the coherent and incoherent components of the target and scatter returns.*

The detection algorithms (2.1), (2.3) are likewise modified here, as a consequence of (2.11), (2.12), to

$$g^{(*)}_{coh} = B^*_{J-coh} - \sum_j l_j < \theta^{(\tau)}_j >, \tag{2.13a}$$

$$g^*_{inc} = B^*_{J-inc} + \frac{1}{2!} \sum_{jj'} (l_j l_{j'} + l'_j \delta_{jj'}) \left[< \theta^{(\tau)}_j \theta^{(\tau)}_{j'} > + < \theta^{(\tau)}_j \theta^{(s)}_{j'} > + < \theta^{(s)}_j \theta^{(\tau)}_{j'} > \right], \tag{2.13b}$$

In order to obtain the "anatomy" of the noise and signal terms in (2.10) we must refer to the propagation models (cf. Secs. III, IV of [1]), from which we see that (in sampled form)

$$n_A = \hat{R}\alpha_A; \quad \theta^{(\tau)}_{direct} = \hat{R}(\alpha_H)_{direct}; \ \theta^{(s)}_{(T \rightarrow S \rightarrow R)} = \hat{R}\alpha_I \tag{2.14}$$

where

$$\alpha_I = (1 - \hat{\eta}_\infty)^{-1} \alpha_H; \quad \alpha_H = \hat{M}_\infty(-G_T); \qquad \hat{\eta} \equiv \hat{M}_\infty \hat{Q}_S \tag{2.14a}$$

in which $\hat{M}_\infty$ is the integral Green's function operator, $\hat{Q}_S$ is the surface inhomogeneity operator and G_T is the (point) source function, which includes the transmitting aperture or array. Here $\hat{R}$ is the receiving aperture or array operator (cf. Sec. II, also, Sec. IV, B of [1]). For surface scatter we may use the results of [1], Section V, Eqs. (34), etc., which give

* We remark that it is possible for $<\theta^{(\tau)}_j \theta^{(s)}_{j'}>$ to be nonvanishing when both $\theta^{(\tau)}$ and $\theta^{(s)}$ have a common specular component, even though signal epoch is not known at the receiver; see Sec. 4.1-2 ff.

in satisfactory approximation. since $\hat{R}$, $\hat{M}_{\infty}$, $\hat{Q}$ are all specifiable in detail [vide [5] and various results below], n_A, etc. are explicitly describable in terms of the propagation physics and geometry. Thus, our attention needs to be directed to the appropriate field forms needed to determine the components of **x**, (2.10). This we shall do in the remaining portions of this document.

2.3 Performance Measures and Bias Terms

Along with the (optimum) threshold detection algorithms summarized in Sec. 2.1 above, we need corresponding performance measures, as well as the bias terms appearing in (2.1), (2.3), (2.4). From [10], Eqs. (4.3a), (4.5a) we write directly, using (2.11), (2.12):

$$B^{*}_{J-coh} = \log\mu - \frac{L^{(2)}}{2}\sum_{m=1}^{M}\sum_{n=1}^{N}\left\{<\theta_j^{(2)}>^2 - <\theta_j^{(1)}>^2\right\}, \quad j = MN;\ j = m,n \tag{2.15a}$$

and

$$B^{*}_{J-inc} = \log\mu - \frac{1}{8}\sum_{jj'}\left\{\left(L^{(4)} - 2L^{(2)^2}\right)\delta_{jj'} + 2L^{(2)^2}\right\}\left[<\theta_j^{(2)}\theta_{j'}^{(2)}>^2 - <\theta_j^{(1)}\theta_{j'}^{(1)}>^2\right]. \tag{2.15b}$$

Furthermore, we have

$$\boxed{\sigma^{*}_{oJ^2} \equiv -2\hat{B}^{*}_{J} = \mathrm{var}_{H_0}\, g^{*}_{J},} \qquad (\mu = p/q;\ q = 1\text{-}p, \text{ or } \mu_{21} = p_2/p_1, \tag{2.16}$$

cf. (68) [1]. This last (without μ) is the key parameter describing binary performance which here is expressed in terms of the usual Neyman-Pearson (N.P.) criterion, as the probability of correctly detection the desired siganl, viz.:

$$P^{*}_{D} \equiv \frac{p}{2}\left\{1 + \Theta\left[\frac{\sigma^{*}_{oJ}}{\sqrt{2}} - \Theta^{-1}\left(1 - 2\alpha^{*}_{F}\right)\right]\right\} \tag{2.17a}$$

with the false-alarm probability

$$\alpha^{*}_{F} \equiv \frac{1}{2}\left\{1 - \Theta\left[\frac{\sigma^{*}_{oJ}}{2\sqrt{2}} + \frac{\log(K/\mu)}{\sqrt{2}\sigma^{*}_{oJ}}\right]\right\} \quad \mu = p/q \tag{2.17b}$$

and K = a preset threshold, compatible with the *a priori* desired value of α^{*}_{F}. [For suboptimum threshold algorithms, cf. (2.2), etc., σ^{*}_{oJ} is replaced by σ_{oJ} formally in (2.17), but different values

for $L^{(2)}$, $L^{(4)}$, cf. (2.18) ff., are required, [10]:

$$L^{(2)} \equiv < l^2 > H_0 \; ; \quad L^{(4)} \equiv < w_1''/w_1')^2 > H_0 \; , \quad < >0 \equiv \int w_1(x|H_0) \, (\,) \, dx. \tag{2.18}$$

In the present extension of our work to include signal-dependent noise, we may now combine (2.11), (2.12) with (2.14), (2.15) in (2.16), to get directly the following general forms of the (threshold) detection performance parameters σ_J^* :

$$\boxed{\sigma^{*2}_{J-coh} = L^{(2)} \sum_j \left\{ < \theta_j^{(\tau)} >^2 + 2 < \theta_j^{(\tau)} >< \theta_j^{(s)} > \right\}} \quad \text{with } s = \sqrt{\psi}\theta, \text{ cf. (2.10b)} \tag{2.19}$$

Depending on geometry $<\theta_j^{(s)}>$ may or may not vanish, cf. (Sec. 4.1-2) ff. Note that $L^{(2)}$, (2.18), is a statistic of the signal-independent noise $n_R + n_A$ only, as in $L^{(4)}$ also. Similarly, for incoherent reception we obtain

$$\sigma^{*2}_{J-coh} = \frac{1}{4} \sum_{jj'} \left\{ \left(L^{(4)} - 2L^{(2)^2} \right) \delta_{jj'} + 2L^{(2)^2} \right\} \left[< \theta_j^{(\tau)} \theta_{j'}^{(\tau)} >^2 + 2 < \theta_j^{(\tau)} \theta_{j'}^{(\tau)} >< \theta_j^{(s)} \theta_{j'}^{(s)} > \right.$$
$$\left. + 2 \left\{ < \theta_j^{(s)} \theta_{j'}^{(\tau)} > + < \theta_j^{(\tau)} \theta_{j'}^{(s)} > \right\} \left\{ < \theta_j^{(s)} \theta_{j'}^{(s)} > + < \theta_j^{(\tau)} \theta_{j'}^{(\tau)} > \right\} + \left(< \theta_j^{(s)} \theta_{j'}^{(\tau)} > + < \theta_j^{(\tau)} \theta_{j'}^{(s)} > \right)^2 \right] \tag{2.20}$$

Again, the $<\theta_j^{(t)}\theta_j^{(s)}>$ cross-correlations may not vanish, particularly if the specular scatter is at all noticiable. This is, of course, strongly dependent on geometry, as we shall see below [cf. Sec. 4.1-2]. From (2.11), (2.20) the critical rôle of the target return is evident.

2.4 An Important Special Case: Preformed Beams

In the case of preformed beams where the detailed array structure is *implicit* in the beam patterns (as in the treatment given in [5]), the spatial sampling of the signal and noise fields by the discrete (m) sensors is now continuous, cf. Appendix II, [5]. As a result the summations Σ_m no longer appear explicitly in our threshold algorithms and perfomance measures, cf. (2.1)-(2.4), (2.14)-(2.20). Thus $\theta_j \rightarrow \theta_n$ here, and we have the equivalent, alternative forms of our earlier theory [9], [10]:

$$\textit{Eq. (2.1)} \rightarrow: \quad g^{(*)}_N(x)_{coh} = B^{(*)}_{N\text{-}coh} - \sum_{n=1}^{N} l_n < \theta_n^{(\tau)} > ; \quad l_n = l(x_n) \tag{2.21}$$

Eq. (2.3) $\rightarrow$:

$$g_J^*(x)_{inc} = B^{(*)}_{N\text{-inc}} + \frac{1}{2!}\sum_{n,n'}(l_n l_{n'} + l'_{n'}\delta_{nn'}) \cdot \left[\langle\theta_n^{(\tau)}\theta_n^{(\tau)}\rangle + \langle\theta_n^{(\tau)}\theta_n^{(s)}\rangle + \langle\theta_n^{(s)}\theta_n^{(\tau)}\rangle\right], \quad (2.22)$$

with corresponding modifications of (2.3a,b,c), i.e., formally dropping "(m)" therein, i.e., J $\rightarrow$ N, j $\rightarrow$ n, etc.

Similarly, the bias terms $\hat{B}$ (2.15a,b) and performance measures (2.19), (2.20) reduce formally to

Eq. (2.15a) $\rightarrow$: $$B^*_{N\text{-coh}} = \log\mu - \frac{L^{(2)}}{2}\sum_{n=1}^{N}\left[\langle\theta_n^{(\tau)}\rangle^2 + 2\langle\theta_n^{(\tau)}\rangle\langle\theta_n^{(s)}\rangle\right] \quad (2.23)$$

Eq. (2.15b) $\rightarrow$: $$B^*_{N\text{-inc}} = \log\mu - \frac{1}{8}\sum_{nn'}\left\{\left(L^{(4)} - 2L^{(2)^2}\right)\delta_{nn'} + 2L^{(2)^2}\right\} \cdot \left\{\langle\theta_n^{(\tau)}\theta_n^{(\tau)}\rangle^2 + 2\langle\theta_n^{(\tau)}\theta_n^{(\tau)}\rangle\langle\theta_n^{(s)}\theta_n^{(s)}\rangle + 2\left[\langle\theta_n^{(s)}\theta_n^{(\tau)}\rangle + \langle\theta_n^{(\tau)}\theta_n^{(s)}\rangle\right]\left[\langle\theta_n^{(s)}\theta_n^{(s)}\rangle + \langle\theta_n^{(\tau)}\theta_n^{(\tau)}\rangle\right]\right\} \quad (2.24)$$

where, by (2.16), σ_N^{*2} and B_N^* are related. The former, by (2.11), (2.12), j $\rightarrow$ n here, become the results below, equivalent to (2.19), (2.20), viz.:

Eq. (2.19) $\rightarrow$: $$\sigma^{*2}_{N\text{-coh}} = L^{(2)}\sum_n\left\{\langle\theta_n^{(\tau)}\rangle^2 + 2\langle\theta_n^{(\tau)}\rangle\langle\theta_n^{(s)}\rangle\right\} \quad (2.25)$$

Eq. (2.20) $\rightarrow$: $$\sigma^*_{N\text{-inc}} = \frac{1}{4}\sum_{nn'}\left\{\left(L^{(4)} - 2L^{(2)^2}\right)\delta_{nn'} + 2L^{(2)^2}\right\} \left\{\langle\theta_n^{(\tau)}\theta_n^{(\tau)}\rangle^2 + 2\langle\theta_n^{(\tau)}\theta_n^{(\tau)}\rangle\langle\theta_n^{(s)}\theta_n^{(s)}\rangle + 2\left[\langle\theta_n^{(s)}\theta_n^{(\tau)}\rangle\langle\theta_n^{(\tau)}\theta_n^{(s)}\rangle\right]\left[\langle\theta_n^{(s)}\theta_n^{(s)}\rangle + \langle\theta_n^{(\tau)}\theta_n^{(\tau)}\rangle\right]\right\}. \quad (2.26)$$

The pertinent results of Sections 3 and 4 ff. are applicable here.

2.5 Analytical Next Steps

The next steps to be taken in our analysis, which are required to give explicit structure to both the bias and performance parameters, cf. (2.16), (2.19), (2.20), are concisely stated. They are:

I. Obtain $\theta_j^{(\$)}$ and $\therefore$ $\langle\theta_j^{(\$)}\rangle$, $\langle\theta_j^{(\$)}\rangle^2$, for *coherent (and incoherent) detection*, cf. (2.19): *"Scatter Signal Models"* (Sec. 3)

II. Obtain ($\theta_j^{(\tau)}$ and $\therefore$ $\langle\theta_j^{(\tau)}\rangle$, $\langle\theta_j^{(\tau)}\rangle^2$, also for coherent detection, cf. (2.14) again: *"Target Models"* (Sec. 4)

III. Construct $\langle\theta_j^{(s)}\theta_j^{(s)}\rangle$, $\langle\theta_j^{(\tau)}\theta_j^{(\tau)}\rangle$, and $\langle\theta_j^{(\tau)}\theta_j^{(s)}\rangle$, cf. (2.20), needed for *incoherent detection.*

Specifically here we shall make the following assumptions:

i. *"narrow band" input signals*;

ii. *far field* (i.e., Fraunhofer) *geometries*;

iii. *Kirchoff theory, and associated approximations*, described in Sec. II, E of [1].

The narrow-band assumption permits analytical solutions for the "signal" terms $\theta^{(s)}$, $\theta^{(\tau)}$ in (2.19), (2.20). (However, at a later stage we may expect to have to consider broad-band cases, where beam patterns, absorption, etc. are frequency dependent and where final results must be obtained computationally.)

Also, for the LPI problem, we shall need to consider the "detection recognition" problem, where the target (now the receiver) does or does not detect the transmittal signal. This formally has the effect of setting $\theta^{(s)} = 0$ and replacing $\theta^{(\tau)}$ in (2.19), (2.20), etc. by θ_j, the received signal (at the target) from the original source (T). As we shall see, this is the simple one-way direct path or "telecommunication model," which does not involve a distributed target configuration [Sec. 5 ff.],* although it does, of course, require an appropriate receiving array, or beam, cf. Secs. 3, 4.

Similarly, for the important case of preformed beams (Sec. 2.4) we parallel I–III above, now for $\theta_j^{(s)} \rightarrow \theta_n^{(s)}$, $\theta_j^{(\tau)} \rightarrow \theta_n^{(\tau)}$.

3. Single Scatter Models, $\theta^{(s)}$

We consdier here first the "classical" cases of *preformed beams* where the details of the array structure are implicit in the resultant beam patterns $\mathcal{A}_T(\nu_o - \nu_{oT}|f_o)$, etc., and correspondingly in the beam pattern projections on the (mean) scattering surface $S_o(x,y)$, e.g., $\mathcal{A}_T \rightarrow \mathcal{A}_T(\mathbf{r},\mathbf{k}_o)$, etc., cf. (17)–(19) vs. (20b), (26) of [5], where $\mathcal{A}_{RT}|_{S_o}$ is the combined beam pattern projection of $\mathcal{A}_T$ and $\mathcal{A}_R$.

In this formulation $\theta_j \rightarrow \theta_n$, cf. Sec. 2.4 above, but the spatial *decorrelation* of the scattered field on S_o can be extensive, i.e., $A_T \sim \Lambda >> \lambda_o^2 \sim \lambda_c^2$, where λ_c is an effective correlation distance of the random surface $\zeta(\mathbf{r},t)$, measured on S_o, and Λ is the effective "illuminated-viewed" surface, vide Fig. 1 of [5]. Thus, the spatial processing gain inherent in spatially independent samples (m) is *implicit* in the beam pattern projections on the scattering surface $S_o(x,y)$, when $\Lambda >> \lambda_o^2 \sim \lambda_c^2$ so that many "independent" scatter samples are available.

---

* If surface scatter is also important, because of source and target geometry, then we may replace θ by $\theta + \theta^{(s)}$, in (2.11), (2.12), (2.19), (2.20), etc.

3.1 Preformed Beams

From (20a), (26) of [5] we have directly for the received scatter signal sample in the scatter geometries described by both Figs. (1.1a,b) and Fig. 1, [5], when multiple scattering (in S_o) is ignored ($l = 0$):

Eq. (20a), [5]:

$$\left.\begin{aligned}\theta_n^{(s)} &= \mathrm{Re}(S_n^{(s)}/\sqrt{\psi}) \\ &= \frac{\tilde{A}_o}{\sqrt{2\psi}}\sigma_n^{(s)}\end{aligned}\right\} \quad \tilde{A}_o \neq A_o$$

$$\therefore\ \theta_n^{(s)} = \mathrm{Re}\left\{\frac{\tilde{A}_o}{\sqrt{2\psi}}\left[\int_{-\infty i+d(=B\tau_1)}^{\infty i+d(\geq 0)} S_{in}(s/2\pi i)F_S^{(o)}(s|\zeta(r,t_n),\ldots)e^{s(t_n-\varepsilon)}\frac{ds}{2\pi i}\right]\right\},\quad t_n = n\Delta t, \tag{3.1a}$$

where $S_{in}(s/2\pi i)$ is the amplitude spectrum of the normalized input signal waveform, to the medium and where $\tilde{A}_o \equiv$ peak value of that signal (which is different from A'_o, (2.16), = peak signal input to receivers.

Eq. (26), [5]:

$$F_S^{(o)} = \sqrt{G^{(1)}}\int_{S_o}\left(\frac{s}{c_o}\right)R_{oS}\,\frac{\mathbf{n}\cdot(\mathbf{i}_{oT}-\mathbf{i}_{oR})}{n_z}\,G_{+S}\;\alpha_{RT(\mathbf{r},k_o)}\cdot$$

$$e^{-(s/c_o)[(r+\zeta)\cdot 2\alpha_o + cT_o]}\cdot e^{-(s/c_o)D_o^{(s)}(v_D/t_n-\varepsilon,r\ldots)}\,dxdy, \tag{3.1b}$$

with

$$dS_o = dydy;\ k_o = \omega_o/c_o = 2\pi f_o/c_o;\ \mathbf{r} = \mathbf{i}_x x + \mathbf{i}_y y \text{ on } S_o;\ T_o = (R_{oT} + R_{oR})/c_o; \tag{3.1c}$$

$$G^{(1)} \equiv e^{-2a\omega_o^2 c_o T_o/(4\pi)^4 R_{oT}^2 + R_{oR}^2} = \text{Eq. (A.1-3)}$$

Here D_o is the doppler (displacement) contribuution from the platforms (T,R), surface drift, deep current, etc. In the present model D_o is found from (24), [17] to be specifically

$$D_o^{(s)} \equiv \underbrace{(2\underset{\sim}{\alpha}_o\cdot\mathbf{v}_c)(t_n-\varepsilon)}_{\substack{\text{volume drift}\\ =\text{"deep current"}}} + \underbrace{(2\alpha_o\cdot\mathbf{v}_d)(t_n-\varepsilon-R_R/c_o)}_{\text{surface drift}} + \underbrace{\{-(\mathbf{i}_{oT}\cdot\mathbf{v}_{oT})(t_n-\varepsilon-T_o) + (\mathbf{i}_{oR}\cdot\mathbf{v}_{oR})(t_n-\varepsilon)\}}_{\text{platform motion}} \tag{3.2}$$

where $\mathbf{v}_c$, $\mathbf{v}_d$, $\mathbf{v}_{oT}$, $\mathbf{v}_{oR}$ are respectively the "deep" or volume current (if any), wind-induced surface drift, and platform velocities. Thus $R_R \equiv R_{oR} - \mathbf{i}_{oR}\cdot\mathbf{r}$, and because here $|r| \ll R_{oR}$ and the dopplers are small, e.g., $|v|/c_o \ll 1$, we can let $R_R \rightarrow R_{oR}$ in D_o, so that *D_o is essentially independent of* $\mathbf{r}$ vis-à-vis the effects of the moving surface, ~$(\mathbf{r} + z)$. In addition, these velocities may have random as well as deterministic components. The velocities themselves, however, are here assumed to be independent of both space and itme variations; (these can be introduced later, when needed).

Also, in (3.1) we have (cf. Appendix A.1 ff.)

$2\underset{\sim}{\alpha}_o = \hat{i}_{oT} - \hat{i}_{oR}$, Eqs. (A.1-3), etc. of [5]; $G^{(1)}$ = Eq. (29b), [5]; (A.1-3) here. (3.2a)

where Fig. 3.1 below shows the directional unit vectors $\hat{i}_{oT}$, $\hat{i}_{oR}$. The wave surface elevation (above S_o) is given by $\zeta(r,t)$ as before. The quantity S_{in} is the *amplitude spectrum* of the normalized input signal waveform $s_n^{(m)} \rightarrow s_n = s(t_n)$, cf. (2.1b) applied at each element (m) of the transmitting array implicitly described by $\mathcal{A}_T$. The first exponential term in (3.1b) represents the path delay and angle modulation in the scattered emissions, caused by the surface motion, while the second contains the effects of any doppler shift and spread, embodied in v_D.

The effects of both transmitting and receiving beam patterns are contained in their joint *projection*, $\mathcal{A}_{RT}|_{S_o}$, on S_o, cf. (3.1b), which may include many correlation distances ($\sim \lambda_c$) of the random wind-wave surface about S_o, cf. the introduction to Sec. 3 above. Appendix A.1 provides definitions of the various other elements of (3.1a,b).

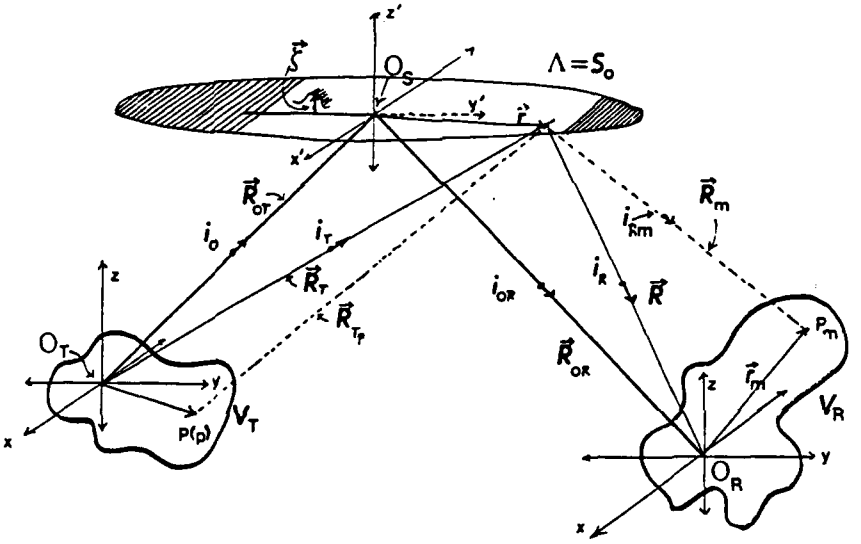

Fig. 3.1. Geometry of transmitter (at O_T), receiver (at O_R), in V_R, and the m^{th} sensor in V_R, in relation to the effective scattering surface Λ, with analogous geometry for the p^{th} sensor in V_T.

For the narrow band signals used here,

$$S_{in}(s/2\pi i) \equiv S_{in}\left(\frac{s-s_o}{2\pi i} = \frac{s'}{2\pi i}\right) \neq 0, \quad |s'| << s_o, \tag{3.3}$$

which allows us to replace s by s' in (3.1a,b), with $e^{s(t_n-\epsilon)} \equiv e^{s_o(t_n-\epsilon)+s'(t_n-\epsilon)}$ in (3.1a) in the usual way, viz.:

$$\theta_n^{(s)}\Big|_{\substack{nn\\ff}} = \mathrm{Re}\left\{ \tilde{a}_o S_o(t_n')_{in}\ \hat{F}_S^{(o)}(ik_o, t_n, \ldots) e^{i\omega_o t_n'} \right\},\ t_n' \equiv t_n - \epsilon - T_o;\ \tilde{a}_o \equiv \tilde{A}_o/\sqrt{\psi}, \tag{3.4}$$

where we have replaced S by s again in (3.1b) also, and where $\hat{F}^{(o)}$ represents (3.1b) now with e^{-sT_o} removed. Here $\hat{S}_o(t_n')$ is the *complex envelope* of the (normalized) driving signal $s(t_n)$, while $\hat{F}^{(o)}$ contains the physical structure of the propagation process. We now note the critical feature of (3.4): *the input signal and the physical structure, $\hat{F}^{(o)}$, are separable, for these narrow-band, far-field cases*, even when the doppler is not independent of position [cf. remarks following (3.2)].

3.2 Arbitrary Arrays—Individual Sensor Elements

We turn next to the important cases of arbitrary arrays, considered on the basis of hte individual (m^{th}) sensor, so that the general algorithmic and performance results of Secs. 2.1–2.3 may be applied directly, when the $\theta_j^{(s)}$, etc. are explicitly obtained.

From Eqs. (30), (31), of [1] we can write for the contribution of the m^{th} receiving sensor to the receiver's input

$$\mathcal{C}_R \rightarrow |A_R^{(m)}(f_o)|\, e^{-i\phi_R^{(m)}(f_o)} \cdot e^{2\pi i(\underset{\sim}{\nu}_{Rm} - \underset{\sim}{\nu}'_{oR})\cdot \mathbf{r}_m}, \tag{3.5}$$

where $\underset{\sim}{\nu}'_{oR}$ ($= \hat{\imath}_{oR} f_o/c_o$) is the (vector) wave number representing the beam steering, as earlier, and where the directional wave number of an elementary scattering source at $\mathbf{r}$, cf. Fig. (3.1) is, namely,

$$\underset{\sim}{\nu}_{Rm} = \hat{\imath}_{Rm} f_o/c_o, \tag{3.6a}$$

$$\hat{\imath}_{Rm} \equiv (\mathbf{R}_{oR} + \mathbf{r}_m - \mathbf{r}) / |\mathbf{R}_{oR} + \mathbf{r}_m - \mathbf{r}|. \tag{3.6b}$$

Using the far-field condition and the fact that the array size ($\sim L_{max}$) and the correlated portions of the scattering surface Λ are small vis-à-vis R_{oT}, R_{oR} allows us to write

$$\hat{\imath}_{Rm} \equiv \hat{\imath}_{oR} - (\mathbf{r}-\mathbf{r}_m) \cdot \frac{\hat{a}_{oR}}{R_{oR}},\ (\text{and } \hat{\imath}_R \equiv \hat{\imath}_{oR} - \mathbf{r} \cdot \frac{\hat{a}_{oR}}{R_{oR}}, \text{ similarly}), \tag{3.7a}$$

where

$$\hat{a}_{oR} = \mathbf{I} - \hat{\imath}_{oR}\hat{\imath}_{oR} \tag{3.7b}$$

is the symmetrical diadic (or 3 x 3 matrix)

$$\hat{\mathbf{a}}_{oR} = \begin{bmatrix} \underset{\sim}{I} - (\hat{i}_{oR})_x^2 & (\hat{i}_{oR})_x(\hat{i}_{oR})_y & (\hat{i}_{oR})_x(\hat{i}_{oR})_z \\ (\hat{i}_{oR})_x(\hat{i}_{oR})_y & \underset{\sim}{I} - (\hat{i}_{oR})_y^2 & (\hat{i}_{oR})_y(\hat{i}_{oR})_z \\ (\hat{i}_{oR})_x(\hat{i}_{oR})_z & (\hat{i}_{oR})y(\hat{i}_{oR})_z & \underset{\sim}{I} - (\hat{i}_{oR})_z^2 \end{bmatrix} \tag{3.7c}$$

whose specific elements are readily obtained from (A.1-2) of [5], etc., for general and monostatic configurations. The (complex) weighting $A^{(m)}$ depends only on the signal's center frequency (f_o).

Our normalized scatter siganl $\theta_j^{(s)}$ now becomes, from (3.1), (3.4), with (3.5), for these n.b. signals, in the far-field régime:

$$\theta^{(s)}_{j=m,n}|_{n.b.} = \mathrm{Re}\left\{\tilde{a}_o \hat{S}_o^{(in)}(t'_n)_{in} e^{i\omega_o t'_n} \hat{F}_S^{(o)}(ik_o, t_n; \ldots)_m\right\}, \quad t'_n \equiv t_n - \varepsilon - T_o, \tag{3.8a}$$

now with (3.5).

$$\hat{F}_S^{(o)}(ik_o|\ldots)_m = \sqrt{G^{(l)}} e^{-ik_o D_o(v_D|t_n-\varepsilon,\ldots)} \cdot \int_{S_o} ik_o R_o S\left(\frac{\hat{n}\cdot(\hat{i}_{oT} - \hat{i}_{oR})}{n_z}\right)_{G+S} \mathcal{A}_T(r,k_o) A_R^{(m)}(f_o)$$

$$\cdot\left[e^{ik_o\{-\hat{i}_{oR} - \hat{i}'_{oR} + r\cdot(\hat{a}_{oR}/R_{oR})\}\cdot r_m} \cdot e^{-ik_o r_m \cdot \hat{a}_{oR}\cdot r_m/R_{oR}}\right] \cdot e^{-ik_o(r+\zeta)\cdot 2\alpha_o} dxdy; \tag{3.8b}$$

$$s \to i\omega_o$$

The exponential term $k_o\{\,\}$ is the brackets [] of (3.8b) is the wave number associated with the steered m^{th} sensor, including radiation from all points (r) on the scattering surface (S_o), while the second exponential contains the correction for the displacement of the m^{th} sensor from the reference O_R, cf. Fig. 3.1. The explicit relations in r_m show how the sensor locations can modify the *Total Surface Scatter Function* (TSSF), $F^{(0)}$, cf. (3.1b), (3.6b). Beam formation here is achieved by summing over (m), e.g., Σ_m, as shown in (2.1), 2.3), and (2,19), (2.20).* Again,

* However, it is clearly not true the $\theta_n = \Sigma_{m,n}$, since $\Sigma_m \langle\theta_{m,n}\rangle^2 \neq \langle(\Sigma_m \theta_{m,n})^2\rangle$, etc., vide (2.14), (2.15), (2.29), (2.30).

the input signal and the physical structure, embodied in the TSSF, $\hat{F}^{(0)}$ here, factor explicitly, cf. (3.4), with D_o given by (3.2) in these cases.

In similar fashion we can "anatomize" the transmitting beam pattern $\mathcal{A}_T$, and write specifically here

$$\mathcal{A}_T = \sum_p |A_T^{(p)}(f_o)| e^{-i\phi_T^{(p)}(f_o)} \cdot e^{2\pi i(\underline{v}_{Tp} - \underline{v}'_{oT})\cdot \underline{r}_p} \Rightarrow \quad a_T(r, k_o), \tag{3.9}$$

this last for the projection of $\mathcal{A}_T$ on S_o, with $\underline{v}'_{oT} = \hat{i}_{oT} f_o / c_o$, the steering wave number, and following (3.4), (3.5)

$$\underline{v}_{Tp} = \hat{i}_{Tp} f_o / c_o; \quad \hat{i}_{Tp} \equiv \hat{i}_{oT} - (\underline{r} - \underline{r}_p \cdot \hat{a}_{oT} / R_{oT}; \quad \hat{a}_{oT} = \mathbf{I} - \hat{i}_{oT} \hat{i}_{oT}, \text{ cf. (3.5c)}, \tag{3.9a}$$

where again we employ the far-field and narrowband conditions. Note that because of these conditions, and the result (19), [5], $\mathcal{A}_T$ necessarily appears as a beam (Σ_p) and thus as a beam projection on S_o, in the TSSF's $\hat{F}_S^{(0)}$ and $F_S^{(0)}{}_m$.

The importance of the "anatomization" of $\mathcal{A}_R$ and $\mathcal{A}_T$, lies in (i) application of specific practical configurations of sensors, and (ii) to beam optimization by direct "matching" of the sensor configuration to the spatial statistics (covariance, usually) of the ambient and scattered fields ([8]; Sec. 10, Sec. 10.4 of [1]; [20], [21]. This incorporation of spatial matched filtering with its venerable temporal analogue (see Sec. 16.3 of [7]), is currently being called "matched field" processing.

3.3 The Mean Scatter Signal $\langle \theta^{(S)} \rangle$

We now carry out the statistical averages denoted by $\langle\ \rangle$, viz.:

$$\langle\ \rangle \equiv \langle\ \rangle_{\varepsilon;\theta'} = [\tilde{a}_o, \zeta, \zeta_{x,y} v_D, \ldots], \tag{3.10}$$

with $\langle\ \rangle_\varepsilon = \int \delta(\varepsilon - \varepsilon_o) d\varepsilon$ and where we use the assumptions and approximations of Sec. 3, [5], namely ζ, ζ_x, ζ_y are independent, as are all the doppler components in (3.2), as well as a_o, etc. Then (3.4) becomes

$$\boxed{\langle \theta_n^{(S)} \rangle = \mathrm{Re}\left\{ \bar{\tilde{a}}_o \hat{S}_o(t'_{on})_{in} \langle \hat{F}_S^{(o)}(t'_{on}) \rangle e^{i\omega_o t'_{on}} \right\}} \qquad t'_{on} \equiv n\Delta t - \varepsilon_o - T_o. \tag{3.11}$$

where now specifically

$$<\hat{F}_S^{(o)}> \equiv ik_o\sqrt{G^{(1)}}\bar{R}_o\bar{S}(-2\alpha_{oz})e^{ik_o\bar{D}_{oc}(t'_{on})}(F_1)\Delta_{v_D}F_1(-k_o2\alpha_{oz})_z \cdot w_{RT}(2k_o\alpha_{o\perp})_S. \qquad (3.11a)$$

The various components of (3.1b) → (3.11a) are:

$$<B(\frac{n \cdot 2\alpha_o}{n_z})> \qquad \equiv -2\alpha_{oz} = b_o = \cos\theta_{oT} + \cos\theta_{oR}, \text{ Eq. (4.2d) and (A.1-3) of [5]}$$
$$\zeta_x\zeta_y:G+S \equiv G \qquad (3.12a)$$

$$<e^{-ik_o\zeta\cdot 2\alpha_o}>_\zeta \qquad = F_1(-2k_o\alpha_{oz})_\zeta, \qquad (3.12b)$$

the (first-order) characteristic function (c.f) of $w_1(\zeta)$, the 1st order pdf of surface elevation, ζ, which is here assumed to be homogeneous, i.e., independent of r;

$$= e^{-R(G\equiv g)/2}, \; Rg \equiv (2k_o\alpha_{oz}\sigma_\zeta)^2, \; \sigma_\zeta^2 \equiv \overline{\zeta^2}, \; <\zeta> = 0 \qquad (3.12c)$$

when ζ is a *gaussian process*, which is a good model here for the large-scale ocean wave surface, cf. (39), (40) of [5]. Thus surface roughness, as is well known, acts to destroy coherence of the scatter signal.

$$e^{-ik_o\bar{D}_{oc}(t'_{on})} \equiv \exp[-ik_o(2\alpha_o\cdot\bar{v}_c)(t'_{on}+T_o)\cdot\exp[-ik_o\{-(2\alpha_o\cdot\bar{v}_d)(t'_{on}+T_oR_{oR}/c_o\}]$$
$$\cdot \exp[-ik_o\{-(\hat{i}_{oT}\cdot\bar{v}_{oT})t'_{on}+(\hat{i}_{oR}\cdot\bar{v}_{oR})(t'_{on}+T_o)\}] \qquad (3.12d)$$

which are the mean doppler components of deep current (v_c), surface drift (v_d), and platform motion $\bar{v}_{oT}$, $\bar{v}_{oR}$:

$$(F1)\Delta v_D \qquad \equiv (F_1)\Delta v_c \cdot (F_1)\Delta v_d \cdot (F_1)\Delta v_{oT} \cdot (F_1)\Delta v_{oR}, \qquad (3.12e)$$

where each $(F_1)\Delta v$ is the c.f. of the fluctuation, Δv, in the various velocities of the present doppler model. Specifically, we have in the case of the usual gaussian pdf's of the Δv's:

$$(F_1)_{\Delta v_C} = \exp\{-ik_o^2(t'_{on}+T_o)^2[(2\alpha_{ox}\sigma_{cx})^2 + (2\alpha_{oy}\sigma_{cy})^2 + (2\alpha_{oz}\sigma_{cz})^2]/2\}, \quad (3.12f)$$

$$(F_1)_{\Delta v_d} = \exp\{-ik_o^2(t'_{on}+T_o-R_{oR}/c_o)^2[(2\alpha_{ox}\sigma_{dx})^2 + (2\alpha_{oy}\sigma_{dy})^2 + (2\alpha_{oz}\sigma_{dz})^2]/2\}, \quad (3.12g)$$

$$(F_1)_{\Delta v_{oT}} = \exp\{-ik_o^2(t'_{on})^2[(2\alpha_{ox}\sigma_{Tx})^2 + (2\alpha_{oy}\sigma_{Ty})^2 + (2\alpha_{oz}\sigma_{Tz})^2]/2\}, \quad (3.12h)$$

$$(F_1)_{\Delta v_{oR}} = \exp\{-ik_o^2(t'_{on}+T_o)^2[(2\alpha_{ox}\sigma_{Rx})^2 + (2\alpha_{oy}\sigma_{Ry})^2 + (2\alpha_{oz}\sigma_{Rz})^2]/2\}, \quad (3.12i)$$

where the $\sigma_{x,y,z}$'s here aare the respective variances of the doppler components. The critical feature of these doppler terms is the progressive degradation of $\langle\theta^{(s)}\rangle$ as the duration (T) of the signal ($\sim\hat{S}_o(t'_{on})$) is increased, a degradation produced by the random doppler fluctuations, Δv, as can be seen directly from (3.12f-i) above. In the limit $T \to \infty$, $(F_1)_{\Delta v} \to 0$, and as expected this doppler "smearing" destroys coherence completely. e.g., $\langle\theta^{(s)}\rangle \to 0$. For "short" signals, of course, this effect can be small, provided the σ's are themselves sufficiently small.

$$w_{RT}(2k_o\alpha_{o\perp})_S = w_{RT}(2k_o\alpha_{ox}, 2k_o\alpha_{oy})_S \equiv \int_{S_o} \mathcal{A}_{RT}(r)e^{2ik_o\underline{\alpha}_o\cdot\mathbf{r}}\mathbf{dr}, \quad \mathbf{dr} = dxdy. \quad (3.12j)$$

This is the (amplitude) *wave number spectrum of the joint beam pattern projections of the reference surface* S_o, with $\alpha_{o\perp}$ the surface components of α_o, since $\mathbf{r}$ has no z-component

For the gaussian beam patterms and projections used in our current model (cf. Appendix II and Eq. (A.2-19) et seq. of [5], where

$$\mathcal{A}_{RT}(\mathbf{r}) = g_{TgR}e^{-k_o^2\mathbf{r}\cdot B_{TR}\cdot\mathbf{r}/2 + ik_o\mathbf{r}\cdot b_{TR}}, \quad (3.12k)$$

(3.12j) becomes, with the help of (A.2-13b),[5],

$$w_{RT}(2k_o\underline{\alpha}_{o\perp})_S = \frac{2\pi g_{TgR}}{k_o^2\sqrt{AB}}\, e^{-\{(2\alpha_{ox}-b_{TRx})^2/A + (2\alpha_{oy}-b_{TRy})^2/B\}/2} \; (= \hat{I}^{1/2}, \text{ Eq. (41), [5]})$$

$$= 2g_{TgR}A_{REF}\exp\{-\tfrac{1}{2}[(2\alpha_{ox}-b_{TRx})^2/A + (2\alpha_{oy}-b_{TRy})^2/B]\}, \quad (3.12l)$$

from (A.3-7) of [5], where $\hat{B}_{TR}$ is the (dimensionless) (2x2) matrix

$$\hat{B}_{TR} = \begin{bmatrix} A & 0 \\ 0 & B \end{bmatrix}, \text{ Eq. (A.2-2) of [5]:}$$

$$A = A_T/R_{0T}^2 + A_R/R_{0R}^2, \quad B = a_T^2 A_T/R_{0T}^2 + b_T^2 A_R/R_{0R}^2 \tag{3.12m}$$

$$b_{TRx} = C; \; b_{TRy} = D$$

cf. A.2-2b of [5] for details, and Eqs. (A.2-19)–(A.2-22) therein; usually $b_{TRx,y} \cong 0$. From (3.12l) is is clear that *unless the beam orientations are essentially in the specular direction*, so that $2\alpha_o - b_{TR} \cong 0$, w_{RT} becomes exponentially small, since A,B are usually also small: *the coherent scatter signal component* $<\theta^{(s)}>$ *also vanishes for "geometrical" reasons.*

3.4 $<\theta_n^{(s)}>^2$

As can be seen from (2.25), we need $<\theta_n^{(s)}>^2$ for the evaluation of detector performance. We readily find from (3.11), (3.12) here that now

$$\boxed{\begin{aligned} <\theta_n^{(s)}>^2 = \; & \frac{1}{2} B_n^{(s)}(t'_{on})^2 \, | \, \hat{S}_o(t'_{on})_{in} \, |^2 \\ & \cdot \{1 - \cos 2 \, [\omega_o t'_{on} - \hat{\Phi}_{in}(t'_{on}) - k_o \bar{D}_o(t'_{on})]\} \end{aligned}} \tag{3.13}$$

where

$$B_n^{(s)}(t'_{on}) \equiv [\bar{a}_o k_o \sqrt{G^{(1)}} \bar{R}_o \bar{S} \; (2\alpha_{oz}) F_1(t'_{on}) \Delta v_D w_{RT}(2k_o \alpha_{o\perp}) e^{-R_G/2}] \tag{3.13a}$$

$$= \{4\bar{a}_o \alpha_{oz} k_o g_T g_R A_{REF} \bar{R}_o \bar{S} \, F_1(t'_{on}) \Delta v_D w_{RT}(2k_o \alpha_{o\perp}) e^{-R_G/2}$$

$$\cdot e^{-\{(2\alpha_{ox} - b_{TRx})^2/A + (2\alpha_{oy} - b_{TRy})^2/B\}/2} \} \tag{3.13b}$$

with

$$A_{REF} = \pi/k_o^2 \sqrt{AB} \text{ , cf. (A.2-33), (A.3-7), [5],} \tag{3.13c}$$

a reference area, used in the definition of scattering cross sections, vide Appendix III of [5]. The

pertinent factors of (3.13a,b) reveal the three components which can degrade the magnitude of the coherent scatter signal: (1) *doppler "smear"* $\sim(F_1)^2_{\Delta v_D}$; (ii) *surface roughness* ($\sim e^{-R_G}$); (iii) *"geometry"* ($\sim w_{RT}$).

Finally, it is important to note that $\hat{F}^{(o)}_S$ and $B^{(s)}_n$ above are independent of the driving or input signal.

3.5 The Scatter Signal Covariance $< \theta^{(s)}_n \theta^{(s)}_{n'} >$

This quantity is essential for the prediction of detector performance in purely incoherent reception, cf. (2.26) above, where $<\theta^{(s)}_n> = 0$. From (32b), [5], we have, generally

$$<\theta^{(s)}_n \theta^{(s)}_{n'}> = \overline{a^2_o}\, G^{(1)}\, k_o^2\, \mathrm{Re}\left\{ \hat{K}_o(\tau)_{in}\, e^{-i\omega_o \tau}\, M^{(o)}_{RT}(\tau|...) \right\} \tag{3.14}$$

where now

$$\hat{K}_o(\tau) \equiv \int_{-\infty}^{\infty} \hat{w}_{in}(f') e^{-i\omega'\tau} df' \; ; \; \hat{w}_{in}(f') \equiv |S_{in}(f')|^2 \, , \quad \tau \equiv (n-n')\Delta t, \tag{3.14a}$$

is the covariance of the normalized input signal envelope waveform, $s(t-\varepsilon,...)$, shifted to $f'(=f-f_o)$ for these narrow band signals, in the manner of (29b,c), [5] and (3.3) above. Note that $K_o(0)_{in} = 1$ here. The quantity $M^{(o)}_{RT}$ is specified by (29d) et seq. of [5], now with the modified doppler term

$$e^{i2\alpha_o \cdot \bar{v}_D k_o \tau} \rightarrow \exp\{ik_o(2\alpha_o \cdot \underline{v}_c + 2\alpha_o \cdot \underline{v}_d - \hat{i}_{oT} \cdot \bar{v}_{oT} + \hat{i}_{oR} \cdot \bar{v}_{oR})\tau\} \tag{3.15}$$

for our present model, cf. (3.2).

This $M^{(o)}_{RT}(\tau)$ becomes generally Eq. (51), [5] for the postulated composite wind-wave surfaces in force here. We have explicitly

$$\begin{aligned} M^{(o)}_{RT}(\tau) \equiv e^{-i2k_o\alpha_o \cdot \bar{v}_D \tau} \cdot \overline{R^2_o S^2} <e^{-i2k_o\alpha_o \cdot \bar{v}_D \tau}>_{\Delta v_D} \\ \cdot \Big[H_G \int_{S_o} \hat{I}_3(\Delta r) F_2(\Delta r, \tau)_G\, e^{2ik_o\alpha_o \cdot \Delta r}\, d(\Delta r) \\ + k_o^2 \int_{S_o} \hat{I}_3(\Delta r) M_{n(0)}(\Delta r, \tau) F_2(\Delta r, \tau)_G M_S(\Delta r, \tau)\, e^{2ik_o\alpha_o \cdot \Delta r}\, d(\Delta r) \Big], \end{aligned} \tag{3.16}$$

which is canonical in the statistics of the surface elevation, ζ_G. $M_{n(0)}$, M_S are respectively the

second-moment functions of the wave "tilt-factors" and the surface soliton component, cf. (49a)–(51). Here H_G has the form

$$H_G \equiv \frac{(\alpha_{ox}^2 + \alpha_{oy}^2 + \alpha_{oz}^2)^2}{\alpha_{oz}/2}, \tag{3.16a}$$

"high-frequency" case, $R_G >> 1$, (3.12c); $= b_o^2 = (2\alpha_{oz})^2$, "low-frequency" case, $R_G \gtrsim 1$; (see Sec. III, D(2) of [5] for details). We have, also,

(A.2-23), [5]:

$$\left.\begin{aligned} \hat{I}_3(\Delta r) &= \int_{-\infty}^{\infty} \mathcal{C}_{RT}(r_1)\, \mathcal{C}_{RT}(r_1 + \Delta r)^* dr_1 \\ &= \frac{\pi g_T^2 g_R^2}{k_o^2 \sqrt{AB}} e^{-k_o^2 \Delta r \cdot \hat{B}_{TR} \cdot \Delta r/4} \cdot e^{-ik_o \Delta r \cdot b_{TR}} \\ &= (g_T g_R)^2 A_{REF}\, e^{-k_o^2 \Delta r \cdot \hat{B}_{TR} \cdot \Delta r/4} \cdot e^{-ik_o \Delta r \cdot b_{TR}}. \end{aligned}\right\} \tag{3.16b}$$

cf. (A.2-30), also (A.2-18)–(A.2-22), [5], specifically for the gaussian beam patterns of (3.12k) and [5]. The (partial) contributions of the "doppler spread" are here

$$\langle e^{-i2k_o \alpha_o \cdot \bar{v}_D \tau} \rangle_{\Delta v_D} = e^{-(2\alpha_o \cdot \sigma_c)^2 k_o^2 \tau^2/2 - (2\alpha_o \cdot \sigma_d)^2 k_o^2 \tau^2/2} \cdot e^{-(l_{oT} \cdot \sigma_T)^2 k_o^2 \tau^2/2 - (l_{oR} \cdot \sigma_R)^2 k_o^2 \tau^2/2} \tag{3.17}$$

where the dependence on τ alone stems from the postulated stationary of the various random processes involved.

In detail, we may distinguish the two important cases of "high-" and "low-frequency" operation. For the former we have from (53), [5] specifically for $M_{RT}^{(o)}$ in (3.14) now

I. "High-Frequency" Cases, $R_G >> 1$:

$$\begin{aligned} M_{RT}^{(o)}(\tau) \equiv e^{2ik_o \alpha_o \cdot \bar{v}_D \tau} \overline{R_o^2 S^2} (g_T g_R)^2 A_{REF}\, e^{-\omega_o^2 \tau^2 (R_\zeta + \sigma_\beta^2)/2} \\ \cdot \left[\left(\frac{(\alpha_{ox}^2 + \alpha_{oy}^2 + \alpha_{oz}^2)^2}{\alpha_{oz}/2} \right)^2 \cdot \frac{2\pi}{k_o^2 b_o^2 \sigma_{Gx} \sigma_{Gy}} e^{-[(2\alpha_{ox} - b_{TRx} + i\alpha_{x\tau}^2 b_o^2 k_o \tau)^2/2b_o^2\sigma_{Gx}^2 + (2\alpha_{oy} - b_{TRy})^2/2b_o^2\sigma_{Gy}^2]} \right. \\ \left. + k_o^2\, e^{-\hat{R}_G \tau^2/2}\, N_{GS-inc}^{(o)}(\alpha_o) W_S(2\alpha_{o\perp} k_o | \tau) \right], \end{aligned} \tag{3.18}$$

where

$$
\left.
\begin{aligned}
R_\zeta &\equiv (b_o\sigma_\zeta/c_o)^2, \text{ Eq. (A.2-19), [5];} \\
\sigma_\beta^2 &= [(2\alpha_o\cdot\sigma_c)^2 + (2\alpha_o\cdot\sigma_d)^2 + (\hat{\imath}_{oT}\cdot\sigma_T)^2 + (\hat{\imath}_{oR}\cdot\sigma_R)^2]k_o^2, \text{ cf. (3.17)} \\
\hat{R}_G &= \text{Eq. (A.8-29b), with (A.8-26a), [5];} \quad b_o = \cos\theta_{oT} + \cos\theta_{oR} = 2\alpha_{oz}, \\
\sigma_{Gx,y}^2 &= \overline{\left(\frac{\partial\zeta_G}{\partial x}\right)^2},\ \overline{\left(\frac{\partial\zeta_G}{\partial y}\right)^2}; \quad \sigma_{x\tau}^2, \text{ (A.8-9a,b) and (A.8-18), [5]}
\end{aligned}
\right\} \tag{3.18a}
$$

$N^{(o)}_{GS-inc}(\alpha_o)$ = {Eq. (48); Appendix IV, A, [5]} is the "tilt factor,"

while

$$W_S(2\alpha_{o\perp}k_o|\tau) = \text{Eq. (54) of [5];} \tag{3.18b}$$

this is the *wave number-time intensity spectrum of the soliton surface ensemble*; vide Appendix IV, B-3,4 also.

For the grazing-angle cases ($\phi_o < 30$: $\theta_{oT} > 60°$), with proper wind conditions [$\bar{U}_\infty \gtrsim$ O(5 m/s)] we get the simpler form of (3.14) explicitly:

$$\boxed{\langle\theta_n^{(s)}\theta_n^{(s)}\rangle = \mathrm{Re}\left\{\hat{B}_o^{(s)}(\tau)_{in}\hat{K}_o(\tau)_{in}\,e^{-i\omega_o\tau}\right\},} \qquad (\phi_o \lesssim 30°) \tag{3.19}$$

where now the "correlation function" $\hat{B}_o$ is

$$\hat{B}_o^{(s)}\big|_{bi} \equiv \overline{a_o^2}\overline{R_o^2}\ \overline{S^2}\ G^{(1)}k_o^4\,(g_T g_R)^2 A_{REF}\,N^{(o)}_{GS-inc}(\alpha_o)e^{2ik_o\alpha_o\cdot\bar{v}_D\tau}\,e^{-\sigma_\Delta^2\tau^2/2}\cdot W_S(2\alpha_{o\perp}k_o|\tau), \tag{3.19a}$$

with a doppler spread

$$\sigma_\Delta^2 \equiv \{\omega_o^2\sigma_\beta^2 + \omega_o^2 R_\zeta + \hat{R}_G\} \tag{3.19b}$$

$\omega_o^2\sigma_\beta^2$: drift, deep current, and platform motion, (3.18a)

$\omega_o^2 R_\zeta$: gravity-wave phase modulation (ϕM), vertical motion (3.18a)

$\hat{R}_G$: AM ($\cong \phi$M) by "tilting" of gravity waves, (3.18a).

The doppler shift ($\sim \bar{v}_D$) is given by (3.15) explicitly. (From (3.14a) we note again that $\hat{K}_o(0)_{in} = 1$). The general effect of $\hat{B}_o(\tau)$, which is comparable in time scale to $\hat{K}_o(\tau)_{in}$, is to "smear," as well as shift, the resulting signal spectrum, and change its level.

II. "Low--Frequency" Cases, $R_G \tilde{<} 1$:

For these cases we use (55a), [5], dropping the "dc" term. The result for (3.14) is now

$$\boxed{<\theta_n^{(s)}\theta_n^{(s)}> = \mathrm{Re}\left\{ \hat{B}_o^{(s)}(\tau)_{lo}\hat{K}_o(\tau)_{in}\, e^{-i\omega_o\tau} \right\},} \tag{3.20}$$

cf. (3.19a), where now, with (49b) and (55c) of [5]

$$\hat{B}_o^{(s)}(\tau)_{lo} \cong \overline{\tilde{a}_o^2}\, \overline{R_o^2}\, \overline{S^2}\, G^{(1)} e^{2ik_o\alpha_o\cdot\bar{v}_D\tau - \omega_o^2\sigma_\beta^2\tau^2/2} (g_T g_R)^2 A_{REF}$$

$$\cdot \left\{ 4A_{REF}\, e^{-(2\alpha_{ox}-b_{TRx})^2/A + (2\alpha_{oy}-b_{TRy})^2/B} + (b_o k_o)^4 W_G(2k_o\alpha_{o\perp}/\tau) \right.$$

$$\left. + k_o^4 N^{(o)}_{GS-inc}(\alpha_o) e^{-\hat{R}_G\tau^2/2} W_S(2\alpha_{o\perp}k_o/\tau) \right\}. \tag{3.20a}$$

The rather different structure of $\hat{B}_o(\tau)_{lo}$ vis-à-vis $\hat{B}_o(\tau)_{hi}$ stems from the behavior of F_{2G} with R_G, cf. (A.8-6,8) vs. 2), Sec. III, E, of [5]. The first term of { } in (3.20a) usually vanishes, unless $2\alpha_{ox}-b_{TRx} \cong 0$, etc., and we are left with the contributions of the large-scale surface waves, which usually dominate, except at very small grazing angles, since $\theta_{oT,oR} \to \pi/2$, or $b_o \to 0$, while $N^{(o)}_{GS-inc} \to 48\,\sigma_{Gy}^4 \sin^4\theta_{oT} > 0$, ($\phi_{oT} = \pi/2$). Again, $\hat{B}_o(\tau)_{lo}$ spreads the spectrum of the received scatter signal. Note, however, that *both* $\hat{B}_o(\tau)_{hi}$ *and* $\hat{B}_o(\tau)_{lo}$ *are independent of the injected signal waveform in these "narrow-band" cases.*

4. Elementary Models of Target Scatter Signals, $\theta^{(\tau)}$

Target modeling from the viewpoint of scattered radiation, like scattering from random ocean surfaces and bottoms, is also a venerable problem. Here we present a short hierarchy of elementary, i.e., *approximate* models, without claiming dominant originality. The main purposes of this hierarchy are (i) to provide specific forms of target signals, $\theta^{(\tau)}$, needed in our analysis of detection performance, and (ii) to indicate some further directions for obtaining realistic target scatter waveforms, which are ultimately required for signal processing applications generally.

Our present and preliminary hierarchy of models may be briefly summarized:

Model I: *Narrow-band signals impinging on a continuous, closed (3-dimensional) acoustic reflecting surface, in the far-field:* This case is readily developed in a formal way, directly from Eq. (3.1a) et seq., above, by some simple, formal modifications of the

directly from Eq. (3.1a) et seq., above, by some simple, formal modifications of the TSSF, $F_S^{(2)}$, (3.1b). See Sec. 4.1 ff. and Fig. 4.1. Evaluation of the integrals, however, presents technical problems.

Model Ia: This is the same formulation as Model I but *with the 3-dimensional surface replaced by a suitably oriented plane scattering surface*, in the manner of Fig. 4.1a.

Model II: Here the continuous, 3-dimensional scattering surface is replaced by *a set of fixed*, but possible randomly located, *reradiating elements ("emitting sensors" in an array)*. The same narrow-band, far-field conditions are assumed here. This is the "discrete facet" or "aligned point scatterer" model.

Model III: This is *Model I*, but *now considered in the Fresnel zone*, as far as phase variations in the incident and scattered radiation is concerned. In this model we can account for "large" distributed targets ($\sim L_{max}$) when the Fraunhofer (far-field) conditions $L_{max}/R << 1$, $2\pi L_{max}\cos\theta_{oT}/\lambda_o << R_{oT,oR}$ (cf. Eq. 19.15 of [23]) are no longer obeyed, i.e., the so-called "bow-aspect."

Model IIIa: This is the partial near field or Fresnel case of *Model Ia*, the plane surface version of Model III.

Model IV: This is the discrete-element version of Model III.

Model Class V: These involve broad-band signals impinging on continuous or discrete reflectors, in the manner of Models I, II above, in the far field.

Model Class VI: This class is the same as that of Model I, but now in the semi near field, or Fresnel phase region. Extensions include the near field effects in the amplitude as well.

All of the models are based, to varying degrees of approximation, on the basic boundary value approach of classical theory [22], [23], of which the Kirchoff or Tangent Plane method is here used primarily [5], for frequencies $O(\geq 0.2$ Hz), cf. remarks in Appendix IV, C, [5].

In addition, because the objects in question are often compliant structures, which can resonate when excited by incident radiation, an additional re-radiation source, with an associated directional beam pattern determined in detail empirically for the type of structure involved, is added to the models above, cf. Sec. 4.4, Eqs. (4.23), (4.24).

Finally, when we are concerned with the passive situation, only the target as possible emitter needs to be considered: this is the well-known "transient" mode, which can usually be ignored in our present concern with the detection of active, reflected sources here. It should be noted, nevertheless, that there are two main ways to proceed with "transient" signals: (1) the simplest is to process the (partially) random class of signal waveforms as seen at the receiver, and (2) the considerably more difficult one, namely, to proceed along the lines of the present analysis (cf. [5]), which require the explicit modeling of both the source and the various media through and in

which the original signal is propagated.

4.1 Target Signal—Model I

This model represents a direct, formal application of our previous result (3.4), starting with (3.1a). Now, instead of a more or less flat, open two-dimensional surface S_o, cf. Fig. 3.1, as scattering element, we replace it with a closed, three-dimensional surface Σ_3, representing our distributed target body. Equation (3.4) is formally modified for the narrow-band signals used here to

$$\theta_n^{(\tau)}\big|_{\substack{n.b.\\ f.f.}} = \mathrm{Re}\left\{ \hat{a}_o \hat{S}_o(t_{\beta n}')_{in}\ \hat{F}_\Sigma^{(o)}(ik_o, t'_{\beta n}, \ldots)_\beta e^{i\omega_o t_{\beta n}'} \right\}, \qquad (4.1)$$

$$t_{\beta n}' \equiv n\Delta t - \epsilon - T_{o\beta};$$

where now, however, $\hat{F}_\Sigma^{(o)}$ is given by [cf. (3.1b)]

$$\hat{F}_\Sigma^{(o)} = ik_o \sqrt{G_\beta^{(1)}} e^{-ik_o D_o^{(\beta)}(v_D, t_{\beta n}')} \int_{\Sigma_3} (R_{\ o} S)_\beta\ (\hat{n} \cdot 2\alpha_{(\beta)})\ \mathcal{O}_{RT}(r_\beta' | f_o)\ e^{-ik_o r_\beta' \cdot 2\alpha_{(o\beta)}}\, d\Sigma_3(r_\beta'), \quad (4.1a)$$

in which the integrand is to be evaluated over the body's surface Σ_3. Here we have for the doppler component (from Eq. (24), [17])

$$D_o^{(\beta)} \equiv (2\alpha_\beta \cdot v_c)(t_{\beta n}' + T_{o\beta}) + (2\alpha_\beta \cdot v_c)(t_{\beta n}' + R_{oT}/c_o)$$

$$+ \left\{ -(\hat{i}_{oT\beta} \cdot v_{oT}) t_{\beta n}' + (\hat{i}_{oR\beta} \cdot v_{oR})(t_{\beta n}' + T_{o\beta}) \right\}, \qquad (4.2a)$$

and

$$r_\beta' = r + \zeta_\beta; \quad r = \hat{i}_r r; \quad \zeta_\beta = \hat{i}_\beta \zeta, \quad \hat{i}_r \cdot \hat{i}_\beta = 0, \qquad (4.2b)$$

so that r and ζ_β are always perpendicular. The directional wavefront normals ($2\alpha_o \rightarrow$) $2\alpha_\beta$ are now $2\alpha_{o\beta} = (\hat{i}_{oT} - \hat{i}_{oR})_\beta$ = Eq. (A.1-3) of [5], where $R_{oT} \rightarrow R_{oT\beta}$, $R_{oR} \rightarrow R_{oR\beta}$, etc., by obvious modification of the geometry of Fig. (3.1), for the ocean wave surface vis-à-vis source and receiver, $\hat{n}$, as before, is an inwardly directed normal to the surface Σ_3. Similarly, $T_{o\beta} = (R_{oT\beta} + R_{oR\beta})/c_o$ is the path time from $O_T \rightarrow O_\beta \rightarrow O_R$; also v_β now is the (constant) velocity of the body, again referred to the fixed reference system $O(x,y,z)_{T,\beta,R}$, with $(|v|/c_o)^2 << 1$, [17]. The geometry of the body system is shown in Fig. 4.1. The quantity $\mathcal{O}_{RT}$, as before, is the projection of the beam pattern on the surface Σ_3; $G_\beta^{(1)}$ is the usual spreading factor, given by (A.1-3), with absorption.

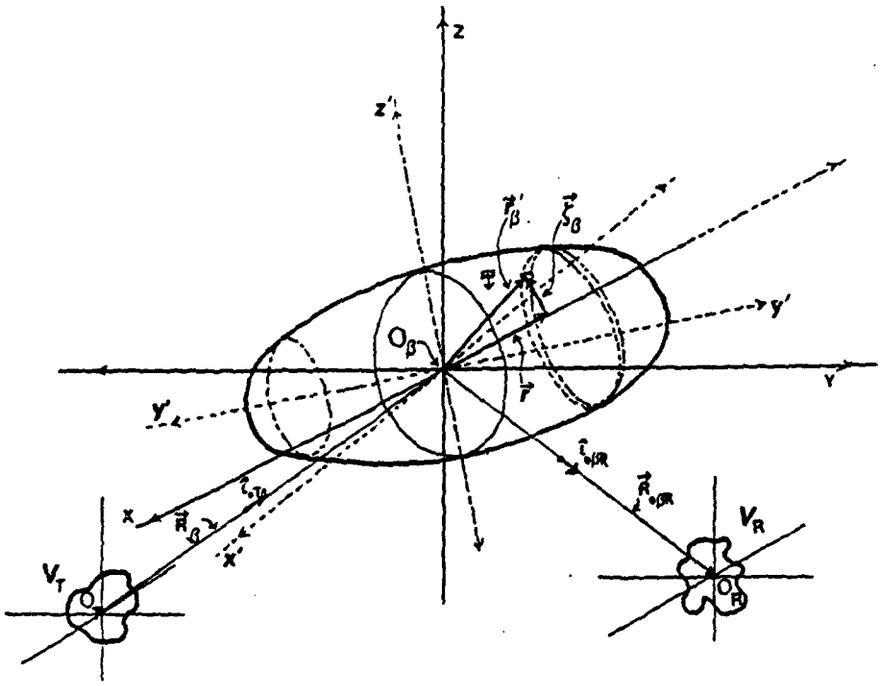

Fig. 4.1: Geometry of the scattering body, vis-à-vis the source (T) and receiver (R), cf. Fig. 3.1.

The critical analytical problem here is the evaluation of the surface integral ($\int \Sigma_3$). This is usually very difficult, so that approximations or numerical methods must be resorted to. In addition, the direction of r (= y), namely, the orientation of the body, is not usually known, and must therefore be regarded as random at the receiver. The quantity $(R_o S)_\beta$ $(\hat{n}\cdot 2\alpha_{(\beta)})$ σ_{RT} can be regarded as the effective beam pattern projection on the now three-dimensional surface Σ_β, analogous to the corresponding situation in the problem of scattering from the wind-wave surface discussed in Section 3, cf. (3.12j). For most bodies $R_{o\beta}$ will be unity (as distinct from water → air → water scattering) cf. [23], pp. 220 et seq.

4.1-1: Coherent Moments of $\theta^{(\tau)}$

The various first- and second-order moments of $\theta_n^{(\tau)}$, needed for optimum threshold *coherent* detection algorithms and performance, cf. Sec. (2.4), can be written down at once from the above (4.1), (4.2), in (3.11), (3.13), namely,

$$\boxed{\begin{aligned} &\langle \theta_n^{(\tau)} \rangle = \mathrm{Re}\left\{ \vec{a}_o \hat{S}_o(t_{on}')_{in} \langle \hat{F}_\Sigma^{(o)}(ik_o, t_{\beta n}) \rangle_\beta e^{i\omega_o t_{\beta n}} \right\}, \\ &t_{\beta n}' \equiv n\Delta t - \epsilon - T_{o\beta}; \end{aligned}} \tag{4.3}$$

where the averages are now

$$< \quad > = < \quad >_{\varepsilon;a_o,i_r,\ldots}, \tag{4.3a}$$

cf. eq. (3.10). The physicogeometric "modulator," $<\hat{F}^{(o)}_{\Sigma}>$, of the original signal becomes

$$<\hat{F}^{(o)}_{\Sigma-\beta}> = ik_o \sqrt{G^{(1)}_{\beta}}\, \bar{R}_{o\beta}\, e^{-ik_o \bar{D}_o(t\beta n')}\, (F_1)_{\Delta v_D} <w_{RT}(2\underset{\sim}{\alpha}_{o\beta}k_o)\beta>_{i_r} \tag{4.4a}$$

where $\bar{R}_{o\beta} \doteq 1$, while $\bar{S}_{\beta} \doteq 1$ (for the surface of the body not "in shadow," as seen by R,T). For the doppler we use (4.2a) in (3.12d–i). The scattering contribution of the body itself is given by *the effective wave number scatter spectrum*

$$<w_{RT}(2\underset{\sim}{\alpha}_{o\beta}k_o)\beta>_{i_r} \equiv \int_{\Sigma_3 \bar{s}\neq 0} <(\hat{n}\cdot 2\underset{\sim}{\alpha}_{o\beta})\, \mathcal{A}_{RT}(r\beta' | f_o)\, e^{-ik_o r\beta'\cdot 2\underset{\sim}{\alpha}_{o\beta}}>_{i_r} d\Sigma_3(r\beta'), \tag{4.4b}$$

where the average is over the body's orientation. This is the quantity, of course, which presents the principal analytical difficulties in evaluation for this model and which prompts us to seek alternative, but valid, approximate forms, cf. Section 4.2 ff.

The analogue of $<\theta^{(s)}_n>^2$, (3.13), here is directly

$$<\theta^{(\tau)}_n>^2 = \frac{1}{2} B_o(t'\beta n)^2_{\beta}\, |\, \hat{S}_o(t'\beta n)_{in}\, |^2 \cdot \{1 - \cos 2\,[\omega_o t'\beta n - \Phi_o(t'_{on})_{in} - k_o \bar{D}_o(t'\beta n)]\} \tag{4.5}$$

where now

$$B_o(t'_{on})\beta \equiv \bar{a}_o k_o \sqrt{G^{(1)}_{\beta}}\, (\bar{R}_o \bar{S})_{\beta}\, F_1(t'_{on})_{\Delta v_D} < w_{RT}(2\underset{\sim}{\alpha}_{o\beta}k_o)\beta>, \tag{4.5a}$$

cf. (3.13a,b). Again, "doppler smear" ($\sim F_{1\text{-}\Delta v_D}$) will degrade (and possibly destroy) the coherent structure of the body scatter. Unlike the wave surface scatter, however, there is no "roughness" degradation here, usually. Finally, note the different path delays ($\sim T_{o\beta}$, etc.) and directionalities ($\sim \alpha_{o\beta}$), etc.: geometry, as always, plays an important rôle.

4.1-2: The Incoherent Moments $\langle \theta_n^{(s)} \theta_n^{(\tau)} \rangle ; \langle \theta_n^{(\tau)} \theta_n^{(s)} \rangle$

From (29), [5] we can write the analogue of (3.14) here as

$$\boxed{\langle \theta_n^{(\tau)} \theta_n^{(\tau)} \rangle = \overline{\hat{a}_o^2}\, G_\beta^{(1)} k_o^2 \, \mathrm{Re} \left\{ \hat{K}_o(\tau)_{in}\, e^{-i\omega_o \tau}\, M_{RT}(\tau)_\beta \right\} .} \tag{4.6}$$

Now (cf. (29d) [5]) and the doppler of (4.2a), with (3.12d)-(3.12i), (3.17) suitably modified gives us

$$M_{RT}^{(o)}(\tau) \equiv e^{-i2k_o \underset{\sim}{\alpha}_o \cdot \bar{v} D\tau} \cdot \overline{R_o^2} \, \langle (e^{-2ik_o \underset{\sim}{\alpha}_o \cdot \bar{v} D\tau} \rangle_{\Delta v_D} \langle W_{RT}(2\alpha_{o\beta} k_o | 0)_\beta \rangle_{\hat{f}_r} \tag{4.6a}$$

in which

$$\langle W_{RT}(2\alpha_{o\beta} k_o | 0)_\beta \rangle_{\hat{f}_r} \equiv \iint_{\Sigma} \langle (\mathcal{O}_{RT}(r'_{1\beta} | f_o) \mathcal{O}_{RT}(r'_{1\beta} + \Delta r' | f_o)^* (\hat{n}_1 \cdot 2\alpha_{o\beta})(\hat{n}_2 \cdot 2\alpha_{o\beta}) \rangle_{\hat{f}_r} \cdot e^{2ik_o \underset{\sim}{\alpha}_{o\beta} \cdot \Delta r'} \, d\Sigma_1(r'_{1\beta}) \, d\Sigma(\Delta r') \tag{4.6b}$$

is the wave number (intensity) spectrum of the scattering body, analogous to (4.4b). Here $\hat{n}_1 = \hat{n}_1(r'_{1\beta})$, $\hat{n}_2 = \hat{n}_2(r'_{1\beta} + \Delta r')$, and $\Delta r'$ always connects two points on the fixed surface Σ: $\Delta r'$ is not random, although r', r are, in direction. Again, a central problem is to evaluate $W_{RT\text{-}\beta}$, (4.6b). Thus, Equation (4.6) can be expressed in the same *form* as (3.19) and (3.20), viz.,

$$\boxed{\langle \theta_n^{(\tau)} \theta_n^{(\tau)} \rangle \doteq \mathrm{Re} \left\{ \hat{B}_o^{(\beta)}(\tau) \hat{K}_o(\tau)_{in}\, e^{-i\omega_o \tau} \right\} ,} \tag{4.7}$$

where the "modulation effects" of the doppler shift and spread, and in particular the scaling by the scatter body (~ $W_{RT\text{-}\beta}$), are described by

$$\hat{B}_o^{(\beta)}(\tau) \doteq \overline{\hat{a}_o^2}\, G_\beta^{(1)} k_o^2\, e^{-2ik_o \alpha_{o\beta} \cdot \bar{v} D\tau}\, \overline{R_o^2} \, \langle e^{2ik_o \underset{\sim}{\alpha}_{o\beta} \cdot \bar{v} D\tau} \rangle_{\Delta v_D} \langle W_{RT}(2\alpha_{o\beta} | 0)_\beta \rangle_{\hat{f}_r} . \tag{4.7a}$$

Specifically, we have for the doppler spread here

$$<e^{2ik_o\alpha_{o\beta}\cdot\bar{v}_D\tau}>_{\Delta v_D} = e^{-\sigma_\Delta^2\tau^2/2};$$

$$\sigma_\Delta^2 \equiv [(2\alpha_{o\beta}\cdot\sigma_c)^2 + (2\alpha_{o\beta}\cdot\sigma_{\beta\beta})^2 + \hat{i}_{oT\beta}\cdot\sigma_T)^2 + \hat{i}_{oR\beta}\cdot\sigma_R)^2]k_o^2. \tag{4.8}$$

from (3.17), where we have replaced $\underline{\sigma}_d$ by $\underline{\sigma}_{\beta\beta}$, the vector spread for the target's motion.

For $<\theta_n^{(s)}\theta_n^{(\tau)}>$, and $<\theta_n^{(\tau)}\theta_n^{(s)}>$, we proceed in a similar way, combining (3.4) and (4.1) and averaging appropriately, according to (4.3a). The result is, finally,

$$<\theta_n^{(s)}\theta_n^{(\tau)}> \doteq \alpha_{oz}\bar{a}_o^2 k_o^2 \sqrt{G^{(1)}G_\beta^{(1)}}\,\bar{R}_o\bar{S}\,\bar{R}_{o\beta}\cdot$$

$$\mathrm{Re}\left\{\hat{K}_o(\tau+\Delta_{o\beta})_{in}\, e^{-i\omega_o(\tau+\Delta_{o\beta})}<w_{RT}(2k_o\alpha_{o\perp})_s\, w_{RT}(2k_o\alpha_{o\beta})_\beta>\cdot<e^{-ik_oD_{01}^{(s)}+ik_oD_{02}^{(\beta)}}>_{\Delta v_D}\right\},$$

$$\Delta_{o\beta} \equiv T_o - T_{o\beta}, \tag{4.9}$$

with $D_o^{(s)}$, $D_o^{(\beta)}$ given respectively by (3.2), (4.2a), and with $\Delta_{o\beta} \to -\Delta_{o\beta}$ and $D_{o1}^{(s)} \to -D_{o2}^{(s)}$, $D_{o2}^{(\beta)}$ $\to -D_{o1}^{(\beta)}$ in (4.9) for $<\theta_n^{(\tau)}\theta_n^{(s)}>$. Here we have as a typical average for the doppler factor* in (4.9):

$$<e^{-ik_o\alpha_o\cdot\bar{v}_c+\Delta v_c t_1 + ik_o\alpha_{o\beta}\cdot\bar{v}_c+\Delta v_c(t_1+\tau)}>_{\Delta v_c}$$

$$= e^{-ik_o\bar{v}_c[t_1\alpha_o-(t_1+\tau)\alpha_{o\beta}]}\cdot F_1(-k_ot_1\alpha_o + k_o(t_1+\tau)\alpha_{o\beta})_{\Delta v_c} \tag{4.9a}$$

where generally $\alpha_o \neq \alpha_{o\beta}$, etc. Thus, when $t_1 \to t_1 + t_o$, and $t_o \to \infty$ for cw signals, not only is (4.9a) representative of a nonstationary process (since dependent explicitly on t_1), but $F_1 \to 0$, in the usual cases where $\Delta v_c \neq 0$. Again, as expected, doppler spread destroys coherence, completely for very long signals, as in the case of $<\theta^{(s)}>$, $<\theta^{(\tau)}>$, (3.11), (4.3) above, also. Even for comparatively short signals doppler spread due to platform and scatter motion can essentially destroy coherence in these far-field situations, because of the long travel times involved, i.e., large R_{oT}/c_o, R_{oR}/c_o, T_o, $T_{o\beta}$, etc., cf. (3.12f-i).

For most practical purposes [unless possibly $\alpha_{o\beta} \doteq \alpha_o$ and $T_{o\beta} \doteq T_o$, which occurs when the target is sufficiently close to the surface scatter domain, cf. Figs. 1.1a,b], *the cross-moments* $<\theta_n^{(s)}\theta_n^{(\tau)}>, <\theta_n^{(\tau)}\theta_n^{(s)}>$ *effectively vanish.* However, even when the target (β) and surface scatter region (S_o) are close, so that $\alpha_{o\beta} \doteq \alpha_o$, $T_{o\beta} \doteq T_o$ are good approximations, the doppler shift

*The epoch (ε) is omitted in there slowly varying terms, since ε is very small, O("RF" cycle): the doppler shift in the envelope $\hat{S}_{o\text{-}in}$ is thus negligible.

and spread terms in (4.9) become explicitly

$$\langle e^{-ik_o D_{01}^{(s)} + ik_o D_{02}^{(\beta)}} \rangle_{\Delta v_D} \doteq e^{ik_o(\bar{v}_c \cdot \alpha_o + \hat{\imath}_{oT} \cdot \bar{v}_{oT} + \hat{\imath}_{oR} \cdot \bar{v}_{oR})\tau}$$

$$\cdot \langle e^{2ik_o \alpha_o \cdot [(\bar{v}_\beta + \Delta v_\beta)(t_1 + \tau + T_{oR}) - (\bar{v}_d + \Delta v_d)(t_1 - T_{oR})]} \rangle_{\Delta v_d, \Delta v_\beta}, \qquad (4.9b)$$

so that unless $\bar{v}_\beta \doteq \bar{v}_d$ *and* $\Delta v_\beta \doteq \Delta v_d$, the doppler spread again destroys coherence between the surface scatter signal and that scattered from the target (β). Our conclusion here, accordingly, is that *for most practical purposes the cross signal moments between surface scatter and the target vanish,** e.g.,

$$\boxed{\langle \theta_n^{(s)} \theta_n^{(\tau)} \rangle \doteq \langle \theta_n^{(\tau)} \theta_n^{(s)} \rangle \doteq 0.} \qquad (4.10)$$

This very considerably simplifies the performance parameter $(\sigma_n^*)_{inc}^2$ in (2.26).

4.2 Model Ia: An Approximate Model I:

The principal approximation here is the replacement of the three-dimensional closed surface Σ_3 of the scattering body of Model I above (Sec. 4.1) by an "equivalent" flat, 2-dimensional scattering surface, in the manner of Fig. 4.2. Then, it is convenient to use the coördinates of the flat target surface to evaluate $w_{RT\text{-}\beta}$, with $S \to \bar{S} \doteq 1$. These coördinates, in turn, need to be related to the primary (parallel) system of O_T and O_R (cf. Fig. 4.1 and Fig. 4.1a). This is done with the help of the familiar rotational transformations ([24], Sec. 8):

	$\hat{\imath}_x$	$\hat{\imath}_y$	$\hat{\imath}_z$
$\hat{\imath}_{x'}$	l_1	l_2	l_3
$\hat{\imath}_{y'}$	m_1	m_2	m_3
$\hat{\imath}_{z'}$	n_1	n_2	n_3

$$\hat{\imath}_{x'} = \hat{\imath}_x l_1 + \hat{\imath}_y l_2 + \hat{\imath}_z l_3$$

$$\hat{\imath}_x = \hat{\imath}_{x'} l_1 + \hat{\imath}_{y'} m_1 + \hat{\imath}_{z'} n_1$$

etc., (4.11)

*This result will not hold, however, in the near field, with signals of short duration, as then the random doppler spread will not have sufficient time to destroy the coherence between the scattering surface and the target.

where l_1, l_2, ... are the direction cosines of $\hat{\imath}_{x'}$, the unit vectors $\hat{\imath}_{x'}$, etc., in the primed system of the "flat" target. Specifically (cf. Fig. 4.1a) we have again (4.2b)

$$\mathbf{r}'_\beta = \mathbf{r} + \underset{\sim}{\zeta}_\beta = \hat{\imath}_r r + \hat{\imath}_\beta \zeta_\beta \; ; \; \hat{\imath}_r \cdot \hat{\imath}_\beta = 0;$$

$$\therefore \quad \mathbf{r}'_\beta = \hat{\imath}_{x'} x' + \hat{\imath}_{y'} y' = \mathbf{r}' \text{ on } \Lambda_\beta$$

$$\text{and} \qquad \hat{\imath}'_z = - \hat{\imath}_{r'} \times \hat{\imath}_\beta = \hat{n} \qquad \text{("inward" drawn normal);}$$

(4.12b)

and in terms of the primary (x,y,z) systems, we get directly

$$(4.13) \quad \begin{cases} \hat{\imath}_\beta = \hat{\imath}_{x'} = \hat{\imath}_x \cos\phi_\beta \sin\theta_\beta + \hat{\imath}_y \sin\phi_\beta \sin\theta_\beta + \hat{\imath}_z \cos\theta_\beta = \hat{\imath}_x l_1 + \hat{\imath}_y l_2 + \hat{\imath}_z l_3, \text{ etc.} \\ \hat{\imath}_r = \hat{\imath}_{y'} = \hat{\imath}_x \cos\phi_r \sin\theta_r + \hat{\imath}_y \sin\phi_r \sin\theta_\beta + \hat{\imath}_z \cos\theta_r \; , \\ \hat{\imath}_r \times \hat{\imath}_r = \hat{\imath}_z = \hat{\imath}_x \{\sin\phi_\beta \sin\theta_\beta \cos\theta_r - \sin\phi_r \sin\theta_r \cos\theta_\beta\} \\ \qquad + \hat{\imath}_y \{\cos\phi_r \sin\theta_r \cos\theta_\beta - \cos\phi_\beta \sin\theta_\beta \cos\theta_r\} \\ \qquad + \hat{\imath}_z \{\cos\phi_\beta \sin\theta_\beta \sin\theta_r - \sin\phi_\beta \sin\theta_\beta \cos\theta_r \sin\theta_r\} \; , \end{cases}$$

where (θ_r,ϕ_r), $(\theta_\beta,\phi_\beta)$ are the respective polar and azimuthal angles of $\mathbf{r}$ and ζ_β in the primary system, cf. Fig. 4.1a. Comparing *the coefficients of* $\hat{\imath}_x$, $\hat{\imath}_y$, $\hat{\imath}_z$ with the relations of (4.11) shows at once that they *are respectively the direction cosine* l_1, *etc.*

From the above it is clear that $w_{RT\text{-}\beta}$ (4.4b) can be evaluated, once $Q_{RT}(\mathbf{r}'_\beta | f_o)$ is specified, since $\hat{n} = \hat{\imath}_z$, so that $(2\alpha_{o\beta})_{z'}$ is readily found to be

$$(2\alpha_{o\beta})_{z'} \cdot (\hat{\imath}_{o\beta T} - \hat{\imath}_{o\beta R}) = \hat{\imath}_{z'} \cdot \mathbf{L}(\hat{\imath}_x, \hat{\imath}_y, \hat{\imath}_z) \qquad (4.14a)$$

where is $\hat{\imath}_{o\beta T} - \hat{\imath}_{o\beta R}$ given by (A.1-3), [5]. Thus, we have with the help of (4.11), in the bistatic cases,

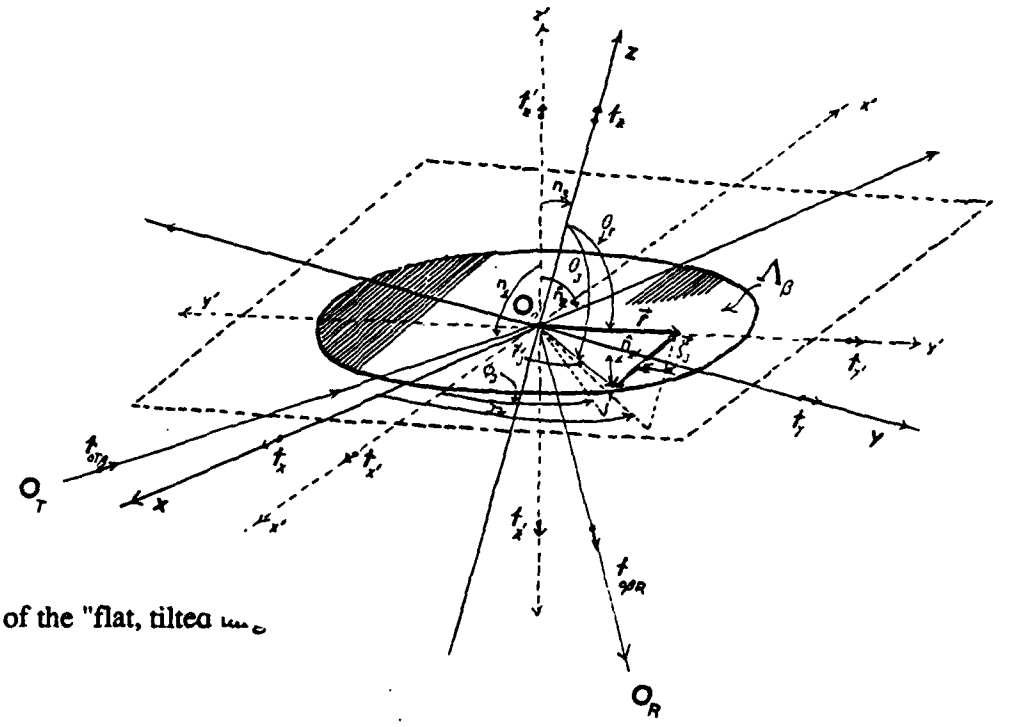

Figure 4.1a: Geometry of the "flat, tilted ...

$$(2\alpha_{o\beta})_{z'} = [\{(1 + R_{oT\beta}/R_{o\beta R})\cos\phi_{T\beta}\sin\theta_{T\beta} - (L_o/R_{o\beta R})\cos\phi_{o\beta L}\}n_1$$

$$+ \{(1 + R_{oT\beta}/R_{o\beta R})\sin\phi_{T\beta}\sin\theta_{T\beta} - (L_o/R_{o\beta R})\sin\phi_{o\beta L}\}n_2 + (\cos\theta_{oT\beta} + \cos\theta_{o\beta R})n_3], \tag{4.14b}$$

with $R_{o\beta R}$ given by (A.1-2c), [5], (with appropriate indexing), *where* n_1, n_2, n_3 *are the coëfficients of* $\hat{i}_x$, $\hat{i}_y$, $\hat{i}_z$ in $\hat{i}_{z'}$, *(4.13) above.* The wave number scatter spectrum $w_{RT\cdot\beta}$, (4.4b) now becomes

$$\langle w_{RT}[(2\underset{\sim}{\alpha}_{o\beta})_{z'}]_\beta \rangle_{\hat{i}_r} = \left\langle (2\alpha_{o\beta})_{z'} \int_{\Lambda_\beta} a_{RT}(\mathbf{r}'|f_o)\, e^{-ik_o \mathbf{r}'\cdot 2\underset{\sim}{\alpha}'_{o\beta\text{-}\perp}}\, dx'dy' \right\rangle_{\hat{i}_r(\theta_o,\phi_o)} \tag{4.15}$$

where $\underset{\sim}{\alpha}'_{o\beta\text{-}\perp} = \hat{i}_{x'}(\alpha_{o\beta})_{x'} + \hat{i}_{y'}(\alpha_{o\beta})_{y'}$, in which the components of $\alpha_{o\beta}$ are readily found from (4.11), (4.13), and the general forms (A.1-3), [5], as done above for $(2\alpha_{o\beta})_{z'}$, (4.14b).

Next, we use (3.12k) for the specific gaussian beam patterns of our current models, with $\mathbf{r} \rightarrow \mathbf{r}'$ (= $\mathbf{r}'_\beta$ here) = $\hat{i}_{x'}x' + \hat{i}_{y'}y'$, cf. (4.12a), and $(\hat{B}_{TR}, b_{TR}) \rightarrow (\hat{B}'_{TR}, b'_{TR})$ for the particular geometry of $T \rightarrow \beta \rightarrow R$ now. All the results for $\langle\theta^{(s)}\rangle$ in Section 3 above carry over directly in

form, with $(2\alpha_{o\beta})_{z'}$ replacing $(2\alpha_o)_{z'}$, etc., and with appropriate modifications of the doppler relations, geometry, etc. See (3.12*l*), (3.13a,b,c), etc. Thus, for this simplified model Ia we have approximate, explicit relations for the various target moments, also with appropriate modifications:

$\langle\theta_n^{(\tau)}\rangle$ = Eq. (3.11), with (3.12), [Eqs. (3.12a,b,c) omitted], (3.12j-m); (4.16a)

$\langle\theta_n^{(\tau)}\rangle^2$ = Eq. (3.13), with (3.13a,b,c); (4.16b)

$\langle\theta_n^{(\tau)},\theta_n^{(\tau)}\rangle$ = Eq. (4.7), with $\langle W_{RT\text{-}\beta}\rangle$, (4.6b), (4.7a), replaced by $\langle W_{RT\text{-}\beta}\rangle$, (4.16c)
(4.17) below, which now for gaussian beam patterns is found to be (without the average over $\mathbf{i}_r$)

$$W_{RT}(2k_o\alpha_{o\beta})\beta = (2\alpha_{o\beta})_{z'}\iint_{\Lambda\beta} \mathcal{A}_{RT}(\mathbf{r}'_1|f_o)\ \mathcal{A}_{RT}(\mathbf{r}'_1+\Delta\mathbf{r}'|f_o)^*\ e^{2ik_o(\alpha'_{o\beta})_\perp\cdot\Delta\mathbf{r}'}d\mathbf{r}'_1 d(\Delta\mathbf{r}'), \quad (4.17)$$

specifically, cf. Fig. (4.1a),

$= (2\alpha_{o\beta})_{z'}\, I_1[(\alpha_{o\beta})_\perp - \mathbf{b}_{RT}/2, (\alpha_{o\beta})_\perp - \mathbf{b}_{TR}/2]$, Eq. (A.2-25), [5] (4.17a)

$= (2\alpha_{o\beta})_{z'}\, 4(g_T g_R)^2 (A'_{REF})^2\, e^{k_o^2(\alpha'_{o\beta})_\perp\cdot\Delta_{TR}\cdot(\alpha'_{o\beta})_\perp}$, (A.2-16), [5] (4.17b)

with $A'_{REF} = \pi/\sqrt{A'B'} = A'_1/2$, and $(\alpha'_{o\beta})_\perp = (\alpha_{o\beta})_\perp - \mathbf{b}'_{RT}/2$. (4.17c)

Similarly, we have for (4.4b) here

$$W_{RT}[2k_o\alpha_{o\beta}]\beta = (2\alpha_{o\beta})_{z'}\int_{\Lambda\beta} \mathcal{A}_{RT}(\mathbf{r}'|f_o)\ e^{2ik_o\mathbf{r}'\cdot(\alpha'_{o\beta})_\perp}\, d\mathbf{r}'$$

= Eq. (3.12*l*,m) $\hat{\mathbf{B}}_{TR} \to \hat{\mathbf{B}}'_{TR}, \mathbf{b}'_{TR}$, etc., in the gaussian cases. (4.18)

With these modifications, then, we get for the cross-averages $\langle\theta_n^{(\tau)},\theta_n^{(s)}\rangle$, etc., Eq. (4.9) with appropriate doppler adjustments in (4.9a,b) and $W_{RT\text{-}\beta}$ given by (4.18):

$\langle\theta_n^{(\tau)},\theta_n^{(s)}\rangle$ = Eq. (4.9), with (4.18), etc., remarks above. (4.19)

Once again, via the arguments of Section 4.1-2 for Eqs. (4.9a), (4.9b), we may expect these cross-averages to vanish, e.g., (4.10) holds here, also, for this simplified model, with

considerable simplification of the performance parameter $\sigma^{(*)2}_{n\text{-}inc}$ (2.26).

Finally, for Model Ia here we also assume, in addition to the far-field conditions, that Λ_β, Fig. (4.1a), is very large compared to the wavelength of the incident radiation, so that "edge effects" may be ignored. (But see our remarks in Sec. 4.3 ff.)

4.3 Model II: "Point-Scatter Model"

Here we replace the continuous plane surface Λ_β of the scattering body by a series of scattering facets (also in the plane Λ_β), whose locations are variable, in the manner of Fig. 4.1b below. This is the "point-scatter" version of Model Ia, whose practical valuation depends on the empirical values we may assign to the various reflection coefficients R_{om} associated with each "facet" about point $\mathbf{r}'_{m\beta}$.

Again, we can write

$$\zeta_m = \hat{\imath}_{x'}\zeta_m;\ \mathbf{r}_m = \hat{\imath}_{y'}r_m;\ \hat{\mathbf{n}} = \hat{\imath}_{z'};\ (\mathbf{r}_m \cdot \zeta_m = 0);\ \ \therefore \hat{\mathbf{n}} \cdot 2\underset{\sim}{\alpha}_{o\beta} = (2\alpha_{o\beta})_{z'}\,. \tag{4.20}$$

Here $\hat{F}^{(o)}_{\Sigma}$, Eqs. (4.1a), (4.4a), apply formally, with $w_{RT\text{-}\beta}$, (4.4b), therein now replaced by

$$w^{(\beta)}_{RT}(2\alpha_{o\beta}k_o)_{discrete} \equiv S\,(2\alpha_{o\beta})_{z'} \sum_{m}^{M} R_{om}\sigma_{RT}(\mathbf{r}'_{m\beta}\,|f_o)\, e^{-ik_o \mathbf{r}'_{m\beta} \cdot 2\underset{\sim}{\alpha}'_{o\beta}}, \tag{4.21}$$

where

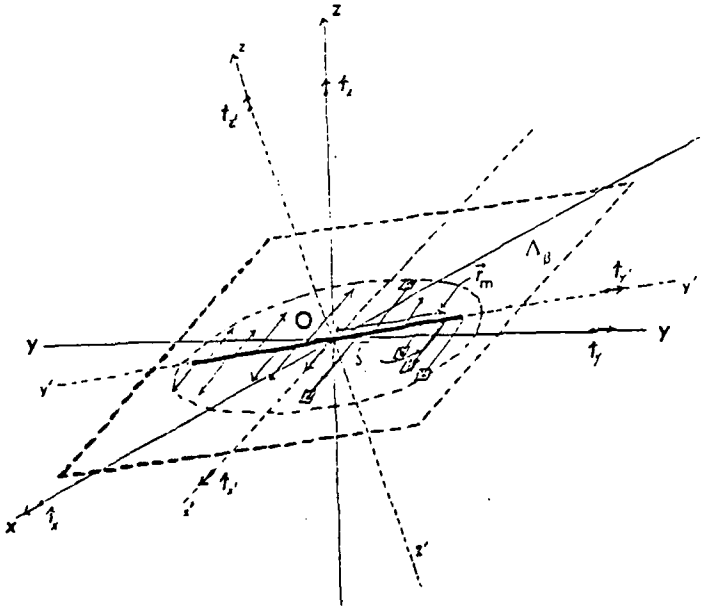

Fig. 4.1b: Point Scatter Target Model

$$\mathbf{r}'_{m\beta} = \hat{\imath}_{x'}\zeta_m + \hat{\imath}_{y'}r_m \tag{4.21a}$$

$$\mathbf{r}'_{m\beta} \cdot 2\underset{\sim}{\alpha}_{o\beta} = (2\alpha_{o\beta})_{x'}\,\zeta_m + (2\alpha_{o\beta})_{y'}\,r_m, \tag{4.21b}$$

with (4.13) specifying the components $\hat{\imath}_{x'}$, $\hat{\imath}_{y'}$, etc. vis-à-vis the basic coördinate system (x,y,z) here, as before. Thus, $w^{(B)}_{RT\text{-}disc}$ is again an effective wave number scatter spectrum of the target body β in this model, which allows us to assign various weights R_{om} (and $\bar{R}_{om}$), as well as various locations along the line y', to each "point"-facet, at $\mathbf{r}'_{m\beta}$.

In a similar way we see that for the second-order moments $\langle\theta^{(\tau)}_n\theta^{(\tau)}_n\rangle$, $\langle\theta^{(\tau)}_n\theta^{(s)}_n\rangle$, etc., cf. (4.6), we have now $(\overline{S}^2 \to 1)$:

$$W^{(\beta)}_{RT}(2k_o\alpha_{o\beta})_{discrete} = (\hat{f}_{z'} \cdot 2\alpha_{o\beta})^2 \sum_{mm'} \overline{R}_{om}\overline{R}_{om'} G_{RT}(r'_{m\beta}\,|f_o) G_{RT}(r'_{m\beta}\,|f_o)^* e^{2ik_o\alpha'_{o\beta}\cdot(r'_m - r'_m)} \tag{4.22}$$

for (4.6a), (4.6b), which may be subject to the further average $< >_{\hat{i}_r=\hat{i}_{y'}}$ as noted above, when target orientation is unknown at the receiver.

The "point-scatter model" as presented here is in part necessarily phenomenological, i.e., we must assign reasonable values to such quantities as R_{om}, $\overline{R_{om}\,R_{om'}}$, r_m, ζ_m, based on empirical studies. Nevertheless, it has the attractive features of (comparative) acoustic simplicity and identification with empirical data. Also, "corner reflector" or "high-light" components may be included, as additional (random) scattering points in Λ_β. We add at once that all this is not a new concept. Our treatment here, however, incorporates a number of features not always included, namely, doppler effects and bi-static configurations with the body β plane, along with source and receiver beam patterns.

4.4. A Resonance Component

In addition to the scattered radiation there may often be a "resonance" component, whereby the scattering body reëmits radiation in a number of "normal" or resonant modes, when the incident radiation is sufficiently intense and consists of short pulses. Here we model the response simply as a *response function*, $Y_o(s)_\beta$, cf. Sec. 2.2-5, 920, [7], associated with an indigenous beam pattern $G_\beta(\nu_\beta\,|f_o)$. Then, this added component, appearing in $\hat{F}^{(o)}_{\Sigma}$, (4.1a) in Models I, Ia, II, is simply

$$Y_o(s)_\beta G_\beta(\nu_{o\beta})\left\{R_{o\beta}\sqrt{G^{(I)}_\beta}\,G_{RT}(r'_\beta)e^{-s_oT_o-(s_o/c_o)(\hat{f}_{o\beta T}\,-\,\hat{i}_{o\beta R})\cdot r'_\beta-(s_o/c_o)D^{(\beta)}_\delta}\delta(r'_\beta-0)\right\}, \tag{4.23}$$

with $(\nu_{o\beta}) = \hat{i}_{x'}f_o/c_o$, cf. (4.2a) for the doppler, where $Y_{o\beta}$ is the narrow-band resonance response, at f_o, of the target, if any, and where G_β is determined by the target structure. This latter quantity must generally be determined empirically and is, of course, a function of orientation ($\hat{i}_{x'}$, (4.13)), which is usually random vis-à-vis the observer.

Accordingly, we must add to $w_{RT\text{-}\beta}$, and $W_{RT\text{-}\beta}$, (4.4b), (4.6b) et seq., the quantity (4.23). We have, then, for Model I:

Eq. (4.4b), $< \theta^{(\tau)} >$: $$<w_{RT\text{-}\beta}>_{\hat{i}_r} \rightarrow \left\{ <w_{RT\text{-}\beta}> + Y_o(s)_\beta G_\beta(\nu_{o\beta}) G_{RT}(0\,|f_o) \right\} \tag{4.24a}$$

Eq. (4.6b), $< \theta^{(\tau)}_n, \theta^{(\tau)}_{n'} >$: $<W_{RT\text{-}\beta}>_{\hat{i}_r} \rightarrow$

$$\left\{ <W_{RT-\beta}> + 2\,\mathrm{Re}\{ <W_{RT-\beta}> Y^{*}_{o-\beta} a^{*}_{\beta} + Y_{o\beta} a_{\beta} a_{RT}(0)^2 \} \right\} \qquad (4.2b)$$

Eq. (4.9), $\langle \theta^{(s)}_n, \theta^{(\tau)}_n \rangle$: $\langle W_{RT\text{-}\beta} \rangle \hat{i}_T \rightarrow$ Eq. (4.24a) (4.24c)

Similarly, $W_{RT\text{-}\beta}$ for Models Ia, II, are modified, cf. (4.15), (4.18); (4.17); (4.21), (4.22), by adding the appropriate "resonance" component, cf. (4.24a-c).

5. The "Telecommunication Model": $T \rightarrow \tau$; $T \rightarrow S \rightarrow \tau$:

In what we call here the "telecommunication" model, because of its analogy to the communication situations in which signals are transmitted directly to the receiver - here on the scattering body (τ) - transmission proceeds as indicated: (i) directly $T \rightarrow \tau$, or (ii) off the ocean surface (S), to the receiver, e.g., $T \rightarrow S \rightarrow \tau$, in the manner of Fig. 1.1b above.

The detection formulation of Secs. 2.3, 2.4 apply here, provided:

(5.1)

Case I, $T \rightarrow \tau$: $\theta^{(\tau)} \rightarrow \theta$; $\theta^{(s)} \rightarrow 0$, in (2.19)-(2.26);

Case II, $T \rightarrow S \rightarrow \tau$: $\theta^{(\tau)} \rightarrow \theta$; $\theta^{(s)} \neq 0$, with receiver R replaced by the body (β), e.g. $O_R \rightarrow O_\beta$, $R_{oR} \rightarrow R_{o\beta R}$, etc.; in the scatter results of Section 3, cf. Fig. 3.1, with corresponding modifications of the doppler, (3.2) et seq.

H_1: $\theta + \theta^{(s)} + N_{amb}$ vs. H_o: N_{amb};

$\theta^{(\tau)} \rightarrow \theta + \theta^{(s)}$ in (2.13a); add $\langle \theta^{(s)}_j, \theta^{(s)}_j \rangle$ in (2.13b);

add $\langle \theta^{(s)} \rangle^2$ in (2.19);

add $\langle \theta^{(s)}_j, \theta^{(s)}_j \rangle^2$ in (2.11)

Case I is the more common situation in practice, although Case II can be important if the receiver is comparatively close to the surface, so that the direct and scatter paths are approximately the same. Then the receiver can use the scatter, or multipath component to enhance detection:

6. Results, Remarks, and Next Steps

Here we briefly summarize the principal results, with comments, and indicate some possible next steps in the analysis:

6.1 Principal Results

In the preceding we have determined

I. *The parameters of the optimum threshold signal detectors* [Secs. 2.1, 2.2], and

II. *The associated parameters for optimum threshold performance* [Secs. 2.3, 2.4], where general nongaussian (plus gaussian) noise is present and when signal-dependent noise is present, produced here primarily by scattering off the ocean surface [Sec. 3]. The results are canonical, i.e., independent of the specific statistics of the ambient (i.e., background) noise, and

are similarly canonical in signal structure.

These results are also quite general: "bistatic" as well as "monostatic" geometries are included. Particular attention is given to the rôle of doppler in the platforms and scatterers.

III. *Target modeling* is explicitly treated (Sec. 4): rather general models are outlined, and approximated by effective two-dimensional (flat) scattering surfaces and point-scatter elements in a plane. These models are quasi-phenomenological, requiring in practice calibration with empirical data.

Throughout we have emphasized realistic structures and have based much of the detailed results on the recent analysis presented in [5], which should be used in conjunction with the present work for the fullest utility. It should be noted, moreover, that in all the cases treated here *the input signal* (envelope) $\hat{S}_0(t)_{in}$, *is explicitly a factor in the parameters describing the threshold algorithms and performance*, either directly, or squared, or in the input signal covariance, cf. (3.4), (3.8a), (3.11), (3.13), (3.14a), (3.19), (3.20), for the signal-dependent scatter, and for the target returns, cf. (4.1), (4.3), (4.5), (4.6), (4.7), (4.9). This explicit and not too surprising separation of the input signal from the physical and geometric factors which embody the scattering mechanisms and their geometries, doppler, etc., is strictly the consequence of the narrow band assumption, in conjunction with the far-field condition, assumed throughout this initial effort. When either or both of these conditions are removed, i.e., broad-band signals and/or Fresnel geometries are invoked, then the present analysis must be appropriately extended: the input signal no longer is factorable from the physico-geometric factors, but appears as a linear functional, either directly as such or as a functional of the signal covariance.

6.2 Next Steps

Various next steps need to be considered. Among them are (not necessarily in the order indicated):

A. *Applications to LPI problems*, with particular attention to the rôle of physico-geometric factors involved in the wave surface and target scattering situations;

B. *Extension of the analysis to the Fresnel region*, in order to account for targets in the beam orientation, where the Fraunhofer condition breaks down;

C. *Calculation of representative results*, for typical geometries;

D. *Quantitative study of the doppler effects*;

E. *Formal extension of the analysis to broad band signals*, as a framework for numerical analysis;

F. *Application of the current results to the estimation of waveform and target level.*

Other important extensions and applications will present themselves in the course of the development of A–F above.

Appendix A.1 Definitions and Descriptions

The principal purpose of this Appendix is to provide definitions of the various terms and elements of Eqs. (3.1a,b), and others, which appear in the text. (Many of these may also be found in Appendix I of [5], as well as in Parts I–III of [6].)

We begin with Eqs. (3.1a,b):

(A.1-1) $F_S^{(\psi)}$ = TSSF = The "Total Surface Spreading Function," Eq. (3.1b), which describes the effects of the random moving wave surface $\zeta(\mathbf{r},t)$ on the incident and scattered acoustic signals

(A.1-2) ε = the signal "epoch," as measured at the receiver

(A.1-3) $G^{(1)}$ $\equiv e^{-2a\omega_o^2 c_o T_o}/(4\pi)^4 R_{oT}^2 R_{oR}^2$, the "geometric" or spreading factor, including the effects of absorption for wave surface scatter

(A.1-4) T_o = $(R_{oT} + R_{oR})/c_o$ = path delay $O_T \rightarrow S(O') \rightarrow O_R$, cf. Fig. 1, [5]

(A.1-5) c_o = (av.) speed of propagation in the water medium

(A.1-6) ω_o = $2\pi f_o$ = carrier signal angular frequency

(A.1-7) R_o = plane wave reflection coefficient for the air-water interface

(A.1-8) S = shadowing function, cf. Appendix IV, [5]

(A.1-9) S_o = Λ = portion of the mean ocean surface jointly "illuminated" by the transmitting and receiving beams, $\mathcal{A}_T$, $\mathcal{A}_R$

(A.1-10) $\hat{\mathbf{n}} \doteq \hat{\mathbf{n}}_G$ = unit normal to the gravity-capillary wave surface, e.g., $\hat{\mathbf{n}} = (\hat{\imath}_x\zeta_x + \hat{\imath}_y\zeta_y - \hat{\imath}_z)n_z$, $\zeta = \zeta_G$; cf. Eq. (23), [5], with $n_z = (1 + \zeta_x^2 + \zeta_y^2)^{-1/2}$

(A.1-11) $\hat{\imath}_{oT}$, $\hat{\imath}_{oR}$ = unit vectors along $\mathbf{R}_{oT}$, $\mathbf{R}_{oR}$, cf. Fig. (1a,b) here and Fig. 1, [5]

(A.1-12) $2\underline{\alpha}_o$ = $\hat{\imath}_{oT} - \hat{\imath}_{oR}$, cf. Appendix I, [5]

(A.1-13) v_D = a doppler velocity, which can include platform motion, surface drift, etc.; cf. Sec. VIII, Appendixes VII, VIII of [5]

(A.1-14) $\int_{Br1}(\ )\frac{ds}{2\pi i}$ = a Bromwich contour (of integration) = $\int_{-i\infty+d}^{i\infty+d(>0)}(\ )\frac{ds}{2\pi i}$, which allows transient or finite duration signal inputs, as well as those of infinite duration ($d \rightarrow 0$)

(A.1-15) V_T, V_R = volumes occupied by the transmitting and receiving arrays, cf. Fig. 3.1.

(A.1-16) $\{---\}_{G+S}$ = quantity [in (3.1b), (3.6b)], associated with the composite surface G (= gravity + capillary waves) and S (= postulated surface soliton ensemble [5], [6]

(A.1-17) $\zeta(\mathbf{r},t)$ = wave surface elevations

(A.1-18) $\hat{\imath}_{o\beta T}$, $\hat{\imath}_{o\beta R}$ = unit vectors along $\mathbf{R}_{o\beta T}$, $\mathbf{R}_{o\beta R}$, cf. Figs. 4.1, 4.1a

(A.1-19) $\hat{F}^{(o)}_{\Sigma_3}$, $\hat{F}^{(o)}_{\Sigma_2}$ = TSSF's for target body (Σ_3), and two-dimensional (flat) target (Σ_2), cf. (A.1-1).

(A.1-20) $G^{(1)}_{\beta}$ = $e^{-2a\omega_o^2 c_o T_{o\beta}}/(4\pi)^4 R_{o\beta T}^2 R_{o\beta R}^2$, "geometric factor" for target, cf. (A.1-3)

(A.1-21) $D^{(s)}_{o}$, $D^{(\beta)}_{o}$ = doppler terms, cf. (3.2), (4.2a), for wave surface and target

(A.1-22) $R_{G,g}$ = Rayleigh numbers

References

[1]. D. Middleton, "Channel Modeling and Threshold Signal Processing in Underwater Acoustics: An Analytical Overview" (Invited Paper), IEEE J. of Oceanic Eng., Vol. OE-12, No. 1, pp. 4–28, Jan., 1987.

[2]. _____, "Statistical-Physical Models of Electromagnetic Interference," IEEE Trans. Electromag. Compatibility, Vol. EMC-19, No. 3, pp. 106–127, Aug., 1977.

[3]. _____, "Canonical and Quasi-canonical Probability Models of Class A Interference," IEEE Trans. Electromag. Compat,, Vol. EMC-25, No. 2, pp. 76–106, May, 1983.

[4]. A. H. Nuttall, I. B. Cohen, and D. Middleton, "Performance Parameters for Quasi-Canonical Class A Non-gaussian Noise: Source distribution law $\mu = 0$, propagation law $\gamma = 2$," Naval Underwater Systems Center (NUSC), New London, CT, Tech. Rpt. 7715, June 15, 1986.

[5]. D. Middleton, "Acoustic Scattering from Composite Wind-Wave Surfaces in 'Bubble-Free' Régimes," (Invited Paper), IEEE J. of Oceanic Engineering, Vol. OE-14, No. 1, pp. 17–75, Jan., 1989.

[6]. _____, "Acoustic Scattering Cross-Sections for Truly Composite Wind-Wave Surfaces: Scattering Without Bubbles" (Part I), NUSC TD-7205, Aug. 20, 1984"; _____, II: Backscatter Cross-Sections and Doppler Effects at High Frequencies and Small Angles for 'Bubble-Free' Régimes," NUSC TR-7635, July 22, 1986; "_____, III: Forward Scattering Intensities and Spatial Coherence at Low and High Frequencies and Small Grazing Angles for 'Bubble-Free' Régimes," NUSC TD-7013, Jan. 23, 1987.

[7]. _____, *An Introduction to Statistical Communication Theory* (McGraw-Hill, New York, 1960); Reprint Edition, Peninsula Publishing Co,. P.O. Box 867, Los Altos, CA 94023, July, 1987–. See in particular here Section 23.2.

[8]. _____, "Active Underwater Acoustic Classification: Some Old Problems and New Approaches in Modeling and Processing," NUSC TR-8067, Aug. 12, 1987. See Sec. 4.4 and pp. 39, 41.

[9]. _____, "Threshold Detection in Non-Gaussian Interference Environments: Exposition and Interpretation of New Results for EMC Applications," IEEE Trans. Electromag. Compat., Vol. EMC-26, No. 1, pp. 19–28, Feb., 1984.

[10]. D. Middleton and A. D. Spaulding, "Optimum Reception in Non-Gaussian Electromagnetic Interference Environments: II. Optimum and Suboptimum Threshold Signal Detection in Class A and B Noise," ITS/NTIA, U.S. Dept. of Commerce, Boulder, CO, NTIA Rpt. 83-120, May, 1983.

[11]. D. Middleton, "Space-Time Processing for Weak Signal Detection in Non-Gaussian and Non-Uniform Electromagnetic Interference (EMI) Fields," ITS/NTIA, U.S. Dept. of

Commerce, Boulder, CO, Contractor Rpt. 86-36, Feb., 1986 (NTIS:PB-86-193406).

[12]. A. D. Spaulding, "Locally Optimum and Suboptimum Detector Performance in a Non-Gaussian Interference Environment," IEEE Trans. Commun., Vol. COM-33, No. 6, pp. 509–517, June, 1985.

[13]. A. R. Milne and J. H. Ganton, "Noise Beneath Sea Ice and Its Dependence on Environmental Mechanisms," U.S. J. of Underwater Acoustics (unclassified paper), Vol. 21, No. 1, pp. 69–80, Jan., 1971.

[14]. R. F. Dyer, "Fram II: Single Channel Ambient Noise Statistics," NUSC TD-6583, Nov. 25, 1981. NUSC, New London, CT 06320.

[15]. R. J. Nielson, F. R. DiNapoli, et al., "TRISTEN/FRAM IV Arctic Ambient Noise Measurements," NUSC Tech. Doc. TD-7133, March 26, 1984, NUSC, New London, CT 06320.

[16]. G. V. Trunk and S. F. George, "Detection of Targets in Non-Gaussian Sea Clutter," IEEE Trans. Aerospace and Electronic Systems, Vol. AES-6, No. 5, Sept., pp. 620–628, 1970. Also, G. V. Trunk, "Radar Properties of Non-Rayleigh Sea Clutter," Ibid., Vol. AES-8, No. 2, March, pp. 196–204, 1972.

[17]. D. Middleton, "Doppler Effects for Randomly Moving Scatterers and Platforms," J. Acoust. Soc. Amer., Vol. 61, pp. 1231–1250, May, 1977.

[18]. _____, "A Statistical Theory of Reverberation and Similar First-Order Scattered Fields. III.," IEEE Trans. Info. Theory, Vol. IT-18, pp. 35–67, 1972.

[19]. D. Middleton and A. D. Spaulding, "A Tutorial Review of Elements of Weak-Signal Detection in Non-Gaussian EMI Environments," NTIA Rpt. 86-194, May, 1986, ITS/NTIA, U.S. Dept. of Commerce, Boulder, CO 80303.

[20]. D. Middleton, "Multiple-Element Threshold Detection of Underwater Acoustic Signals in Nongaussian Interference Environments," Contractor Rpt. 231, 18 May 1984, Naval Ocean Systems Center (NOSC), San Diego, CA 92152. See also Vol. 2: "Studies in Acoustic Signal Processing," 1987, in the series: *Scientific and Engineering Studies*, Naval Underwater Systems Center (NUSC), New London, CT 06320.

[21]. _____, "Threshold Vector Field Detectors," IEEE Trans. Electromag. Compatibility, Vol. 30, No. 4, pp. 538–552, Nov., 1988.

[22]. P. M. Morse and H. Feshbach, *Methods of Theoretical Physics*, New York (McGraw-Hill), Chapters 6,7, 1953.

[23]. F. G. Bass and I. M. Fuks, *Wave Scattering from Statistically Rough Surfaces*, C. B. Vesecky and J. F. Vesecky, Eds. and Translators, New York (Pergamon), 1979. Chapters 1, 7, esp.

[24]. L. Page, *Introduction to Theoretical Physics*, D. Van Nostrand (New York), 2nd ed., 1935.

INITIAL DISTRIBUTION LIST

Addressee	No. of Copies
CNA	1
CNR	
OCNR-00	1
R. F. Obrochta (Code 1125 AR)	1
Dr. B. R. Junker (Code 111)	1
Dr. R. N. Madan (Code 11145E)	1
E. Hartwig (Code 1122B)	1
Dr. J. Abrahams (Code 1111 SP)	1
Dr. N. Gerr (Code 1111)	1
Dr. T. B. Curtin (Code 1125 AR)	1
NRL	
Dr. L. Wetzel (Code 5303)	1
Dr. E. Franchi (Code 5160)	1
Dr. J. S. Perkins	1
Dr. A. Tolstoy	1
NAVSEA	
CDR E. Graham (SEA 63-D)	1
NORDA, Bay St. Louis	
Code 530	1
Dr. R. Farwell	1
Dr. M. Y. Su	1
B. Adams (Code 113)	1
Dr. N. Kinney	1
Dr. S. A. Chin-Bing	1
Dr. M. F. Werby	1
T. Goldsberry	1
NOSC, San Diego	
Dr. E. Cooper (Code 013)	1
Dr. J. Northrup (Code 5322)	1
Dr. F. Spiess	1
Dr. C Persons (Code 7133)	1
B. Smith	1
Dr. H. Bucher	1
ITS/NTIA	
Dr. A. D. Spaulding	1
Dr. C. Rush	1
APL, UNIV OF TEXAS AT AUSTIN	
Dr. G. Wilson	1
G. Ellis	1
Dr. R. Culbertson	1
Dr. H. Boheme	1
DTIC	12
DARPA	
Dr. R. Repka	1
Dr. A. Ellinthorpe	1
ONT	
Dr. R. Doolittle	1

INITIAL DISTRIBUTION LIST (CONT'D)

Addressee	No. of Copies
NPS	
Superintendent	1
Prof. H. Medwin	1
Prof. J. Wozencraft	1
NSWC	
Dr. G. C. Gaunaurd (Code R-43)	1
SCRIPPS INSTITUTE OF OCEANOGRAPHY	
Dr. F. Fisher	1
ROYAL AEROSPACE ESTABLISHMENT	
Dr. M. J. Buckingham	1
ARL, PENN STATE	
Dr. D. McCammon	1
Dr. F. Symon	1
Prof. S. T. McDaniel	1
NOAA, Boulder, CO	
Dr. V. E. Derr, Dir	1
Dr. S. Clifford	1
SACLANT ASW RES CTR	1
RAYTHEON, Portsmouth, RI	
S. Ehrlich	1
J. Bartram	1
RAYTHEON, Res Div, Lexington, MA	
Dr. J. A. Mullen	1
Dr. R. Price	1
YALE UNIV	
Prof. P. H. Schultheiss	1
SAIC	
W. L. Chadsey	1
Dr. J. Brackett-Hersey	1
Dr. Tatrow	1
Dr. R. Green	1
SAI - SPACE SYS OPER	
Dr. R. Becherer	1
CYBERLINK	
Dr. P. McManamon	1
APL, JOHNS HOPKINS, Laurel, MD	
Dr. J. Apel	1
JOHNS HOPKINS UNIV, Baltimore, MD	
Prof. O. M. Phillips	1
UNIV OF WISCONSIN	
Prof. C. S. Clay	1
UNIV OF MIAMI	
Dr. F. D. Tappert	1
APL, UNIV OF WASHINGTON	
Dr. E. Thorsos	1
Dr. D. R. Jackson	1
Dr. S. McConnell	1

INITIAL DISTRIBUTION LIST (CONT'D)

Addressee	No. of Copies
UNIV OF WASHINGTON, Dept of Elec Engineering	
Prof. A. Ishimaru	1
UNIV OF CALIF AT SAN DIEGO	
Dr. W. Munk	1
Prof. C. Helstrom	1
UNIV OF CALIF AT SANTA BARBARA	
Prof. M. Tulin	1
SONALYSTS, INC	
W. N. Pugliese	1
KILDARE CORP	
Dr. R. H. Mellen	1
J. W. Fitzgerald	1
PRINCETON UNIV	
Prof. S. Schwartz	1
GEORGE MASON UNIV	
Prof. E. Wegman	1
UNIV OF RHODE ISLAND	
Prof. D. Tufts	1
Prof. S. Kay	1
RICE UNIV	
Prof. R. de Figuereido	1
MIT	
Prof. A. Baggeroer	1
Prof. J. A. Kong	1
Prof. I. Dyer	1
BOLT, BERANEK, & NEWMAN, Arlington, VA	
Dr. H. Cox	1
BOLT, BERANEK, & NEWMAN, New London, CT	
J. Hanrahan	1
Dr. P. Cable	1
SELENIA, S.p.A.	
Dr. R. Esposito	1
GENERAL MOTORS RESEARCH LAB	
Dr. R. A. Frosch	1
SOUTHWEST RESEARCH INSTITUTE	
M. Goland	1
THE RAND CORP	
Dr. E. Bedrosian	1
SRI INTERNATIONAL	
Dr. O. G. Villard, Jr.	1
STANFORD UNIV	
Prof. B. Widrow	1
Prof. J. W. Goodman	1
UNIV OF SOUTHERN CALIFORNIA	
Prof. I. S. Reed	1
WOODS HOLE OCEANOGRAPHIC INSTITUTION	
Dr. T. K. Stanton	1

INITIAL DISTRIBUTION LIST (CONT'D)

Addressee	No. of Copies
HARVARD UNIV	
Prof. G. Birkhoff	1
BROWN UNIV	
Dr. R. Beyer	1
VIRGINIA POLYTECHNIC INSTITUTE	
Prof. I. M. Besieris	1
NORTHEASTERN UNIV CORP	
Prof. H. R. Raemer	1
IDA–CRD	
Dr. D. I. Lieberman	1
Dr. J. DeLucia	1
IDA–SRC	
Dr. P. Schneck	1
Dr. H. Freitag	1
IDA, Alexandria	
Dr. R. D. Turner	1
LAB FOR PHYSICAL SCIENCES	
Dr. T. Beahn	1
UNIV OF ARIZONA	
Prof. J. R. Wait	1
UNIV OF CAMBRIDGE, Cambridge, England	
Dr. B. J. Uscinski	1
Dr. B. Kerman	1
Prof. Longuet–Higgins	1
MULTIFLOW COMPUTER, INC	
Dr. C. Pangali	1
DEFENCE RESEARCH ESTABLISHMENT	
Dr. M. F. Chapman	1
DR. D. MIDDLETON, New York	25
DR. A. O. SYKES, Vienna, VA	1
DR. M. SCHULKIN, Potomac, MD	1
DR. D. HOLLIDAY, Sacramento, CA	1
DR. D. P. PETERSEN	1
DR. W. A. VON WINKLE	1